Model predictive control of anaerobic co-digestion: experimental validation of a robust tube-based scheme: Supplementary Material

D. Carecci, L. Dewasme, E. Ficara, A. Vande Wouwer, G. Ferretti, S. García-Gen

In the following, some further methodological details and result materials are reported, as referenced in the text of the main manuscript. Section I reports a brief yet comprehensive literature review of state estimation and model-based control of the AcoD process. Section II extensively describes both high-fidelity (agri-AcoDM) and reduced-order ($AM2HN_{tan} \rightarrow AM2HN_{obs}$) models. Details about feedstocks' characterization, EKF formulation, the selector-PI algorithm, NMPC control law/design parameters and details about practical closed-loop implementation of the real bench-scale facility are reported too. Further results about models' performances, EKF tuning, the comparison between the two controllers and practical observability are reported in Section III.

In the tables, a minor notation simplification is adopted, whereby e^a is used in place of $\times 10^a$ for each a exponent for the sake of readability.

Vectors in $\mathbb{R}^m$ (e.g., $\mathbf{COD_{X_h}/VS_{X_h}}$, $\mathbf{k_h}$ and $\mathbf{X_h}$) are ordered as maize silage, cow slurry, tomato sauce. Accordingly, index (1) refers to maize silage, (2) to cow slurry, and (3) to tomato sauce.

For ease of interpretation of tabulated and plotted values, the following approximate conversions may be used: (i) gaseous flow rates can be converted from mmol L^{-1} d^{-1} to L_{GAS} $L_{REACTOR}{}^{-1}$ h^{-1} dividing by $\simeq 39$; (ii) TVFA can be converted from mmol L^{-1} to g_{COD} L^{-1} by multiplying by 0.06.

I. Literature review

A. State observer

In literature, many state observer's designs have been proposed for the AD process, but, coherently to the suggested controllers, the vast majority focuses on the AM2 model and/or misses experimental validation [8], [9], [18], [19], [37], [42], [43], [45], [53], [54], [62], [64], [66]. Among the works that resulted from the Scopus database[1], some conducted experimental validations, but mainly in the case of the mono-digestion of simple/easily biodegradable feedstocks [3]–[5], [20], [22], [29], [33], [43], [46], [52], [60]. Only two studies departed from the exploitation of the AM2 model, by proposing Unscented Kalman Filter (UKF)-based observers for case studies close to the one of interest in the current work (a hydrolysis-extended AM2 [58] and the ADM1-R4 model [36]), but without experimental validation.

For the cases of interest, the main issue preventing the application of the AM2-based state observers developed in literature is that they rely on the assumption of *online* measurability of the biodegradable soluble organic matter (S_1) and TVFA (S_2) concentrations (e.g. [3]–[5], [18], [19], [29], [37], [46], [52]–[54], [60], [62], [64], [66]); however, this hypothesis holds true for the mono-digestion of simple/easily biodegradable feedstock only, whereas it does not for plants fed on complex agro-industrial feedstocks, where such quantities cannot be measured at all or at least with a frequency consistent with the system's characteristic time of response (i.e., *online*). Indeed, as an example, even though the adequacy of automatic titration-based data (e.g. IA/TAC or FOS/TAC) for general monitoring purposes is undoubted (e.g. IA/TAC ratio proved to be a reliable indicator of stability against acidification in co-digestion experiments [26]), these cannot be employed as a reliable proxy for S_2 if the presence of other weak acids is relevant (since amino acids, lactic and succinic acids, and humic substances exhibit dissociation constants within the same pH range of VFAs).

On the other hand, the proposals that consider methane flow rate (q_M) as the only *online*-available data, limit the process model to the sole two-step reactions' core of the original AM2 model, i.e. two microbial groups (acidogens X_1, methanogens X_2) and their respective substrates (S_1, S_2), for reasons rooted in the model's observability (e.g. [9], [20], [22], [33], [42], [43], [45]). To model the pH and the CO_2 gas flow rate (q_C) dynamics (exploiting the availability of such measurement for model training and validation), the inclusion of the dissolved inorganic carbon (C) and total alkalinity (Z) state variables was required and considered in the original AM2 model version. However, Attar *et al.* [8] verified that the gas data only (q_M and q_C flow rates) are not sufficient to provide full observability for the original AM2 model (5 states out of 6 are observable), while it is reached when the pH data are considered too. This result was exploited by Raeyatdoost *et al.* [58] to design an UKF for an AM2HN-like model applied to the mono-digestion of the organic fraction of municipal solid waste (OFMSW). Unfortunately, pH is not reliably measurable *online* in the full-scale plants of interest (due to fouling, clogging, and rapid calibration drift for electrodes directly inserted in the digesters).

[1] seeking for: *anaerobic AND digestion AND state AND (observer OR estimator OR estimation)* in the "Title, Keywords, Abstract" sections.

B. MPC

As suggested in the main manuscript, seeking for contributions in the field of MPC[2], literature is very poor in proposals applied to the AcoD process and/or experimentally validated (see Table S1).

TABLE S1: Main literature contributions about MPC applied to AD/AcoD systems.

Reference	Diet	Exp.valid.	Model	State observer	Notes
Aceves-Lara *et al.* 2010 [1]	AD of molasses	Yes, lab-scale	Non-linear ODE system; glucose metabolism (one-step* model)	Asymptotic observer	H_2 production from a soluble/easily biodegradable feedstock.
Haugen *et al.* 2014 [33]	AD of diluted and sieved dairy manure	Yes, big pilot-scale (UASB)	Simplified Hill's model	UKF	Neither hydrolysis nor VFA inhibition in the model. Simple NMPC optimization problem.
Xue *et al.* 2015 [74]	AcoD of maize silage and swine manure	No	Multiple-step simplified ADM1 (from sensitivity analysis)	UKF	Not clear which are the hypothesis on measurements' availability.
Mauky *et al.* 2016 [48]	AcoD of maize silage and cattle manure	Yes, agro-industrial AcoD full-scale	Single-step model from the ADM1 simplification carried out by Weinrich *et al.* [70] (simplified ADM1-R4)	Missing*	Maize silage daily feeding is the only manipulated variable. Goal of matching a demand-driven production. *Recursive parameter update included in the control scheme, but, to the best of the authors' understanding, state observer missing
Kil *et al.* 2017 [38]	AD of soluble and particulate substrates	No	Reformulated AM2-core to avoid microbial concentration as states*; includes N release to alkalinity	Recursive three-step filter (RTSF) and EKF*	Hypothesize biodegradable soluble COD and TVFA *online*-measurability. *Maximum rates of acidogenic and methanogenic degradation as states, estimated recursively *online*, along with process rates and yield coefficients.
Ahmed *et al.* 2020 [2]	AD of glucose	No	Two-step modified AM2 with hydrogenotrophic methanogenesis	Semi-mechanistic estimator*	Hypothesize pH, biodegradable soluble COD and TVFA *online*-measurability. Unrealistic availability of alkali solution supplement as manipulated variable. *Relies on 48h-delayed *offline* data of methanogens concentration.
Piceno-Díaz *et al.* 2020 [55]	AD of tequila vinasses	No	AM2	Missing*	Two-step AD. Robust multi-scenario NMPC to deal with uncertainty in kinetic process parameters. *Hypothesize unrealistic state-feedback.
Yoshida *et al.* 2020 [75]	AcoD of food and paper wastes	Yes, pilot-scale	Single-step linearized state-space data-driven model	Not needed	Goal of a demand-driven production. Trapezoidal setpoint followed manipulating the OLR. Recursive parameter update included in the control scheme.
Ghanavati *et al.* 2021 [28]	AD of waste activated sludge (WAS)	No	Linear data-driven models (Auto-regressive moving average (ARMA))	Not needed*	Recursive parameter estimation (adaptive ARMA). Two MPCs with override combined with a fuzzy reference governor to maximize biomethane only when operations are considered safe (TVFA values are below a certain threshold). *Relies on the unrealistic *online*-measurability of TVFA.
Li *et al.* 2021 [44]	AcoD of food waste, swine slurry and waste sludge	Yes, lab-scale	Linearized version of the ADM1 (LADM1)	Missing*	Two-step AD. Comprehensive modeling effort, but control problem not extensively described. *To the authors' understanding, controller operated in an open-loop fashion (mainly to validate the model predictive ability)
García-Gen *et al.* 2021 [27]	AcoD of sewage sludge and pig manure	Yes, bench-scale	ADM1*	Missing*	Control of OLR, HRT, diet composition. Manual feeding (control interval of 5 days, too long to cope with possible intermediate rise of inhibitions). *Linear programming combined with open-loop ADM1 (extended to AcoD) predictions to optimize OLR after diet mix is defined by the linear program.
García-Gen *et al.* 2022 [25]	AD of wine distillate waste	No	AM2	Missing*	Control of biomethane flow to reference variable setpoint. *Preliminary study under hypothesis of full-state knowledge.
Cortés *et al.* 2022 [19]	AD of tequila vinasses (distillery effluent)	No	Extended AM2 with N release to alkalinity	Asymptotic + Reaction rate observers	Hypothesize biodegradable soluble COD and TVFA *online*-measurability.
Körber *et al.* 2022 [41]	AcoD of maize silage, shredded sugar beets, cattle slurry	Yes, small pilot-scale	Same as Mauky *et al.* 2016 [48]	Same as Mauky *et al.* 2016 [48]	Flexible biogas production designed to cover the residual electricity load of a self-sufficient community.

[2]seeking for: *anaerobic AND digestion AND model AND predictive AND control* in the "Title, Keywords, Abstract" sections.

Tawai *et al.* 2022 [66]	AD of winery wastewater	No	AM2	Nonlinear state observer	Two-step AD. Hypothesize biodegradable soluble COD and TVFA *online*-measurability. Analytical Model Predictive Control (AMPC) based on input-output linearization (adaptive optimal setpoints).
He *et al.* 2023 [34]	AD of cellulose	No	Linear data-driven model (Ultra-Local Model (ULM))	Not needed*	Two-step AD. ULM to approximate the complex system in a short time sliding window. *Time-Delay Estimation (TDE) to observe unknown disturbance.
Bai *et al.* 2024 [10]	AcoD of food and paper waste, sieved cattle slurry	Yes, fed-batch small lab-scale	Linear data-driven model (Multivariable Output Error State Space (MOESP))	KF	Control of the overall biogas flow rate to a setpoint. 21–days experiment: apparently, not very good tracking results.
Azúa-Poblete *et al.* 2025 [9]	Readily biodegradable soluble wastes	No	AM2-core	EKF	Exogenous EKF augmented with additional unknown disturbance estimation for offset-free biomethane flow rate tracking.
Pino Santana *et al.* 2025 [56]	AD of synthetic composition	No	Nonlinear data-driven model (long short-term memory (LSTM))	Not needed	–
Hellman *et al.* 2026 [35]	AcoD of maize, grass and sugar beet silages, cattle manure	No	Single-step model from the ADM1 simplification carried out by Weinrich *et al.* [70] (ADM1-R3)	Missing*	Robust multi-stage NMPC to deal with uncertainty in influent composition. *Recursive parameter update included in the control scheme, but state observer missing.

**Note that* step *in this context refers to the number of steps used to schematize the AD process.*

Compared with AD, considerably less attention has been devoted in the literature to the modeling and model-based control of AcoD systems [50], [73]. Despite the well-known partial observability of the ADM1 model, Gaida *et al.* [23] developed a state estimator for such model, based on various machine learning techniques and the sole measurement of pH, gas flow rate and composition. The estimator was then used along with a NMPC controller in a simulation study [24] applied to the AcoD of maize silage, cattle slurry and manure, but the experimental validation is missing. Zhou *et al.* [76] proposed a strategy in which feed ratio is regulated by a PID controller and setpoints are updated through TVFA/TAC-based rules; however, the approach was validated in simulation only. Putra *et al.* [57] employed a simple SISO state-space (linear second-order input-output model) and PI controllers (rather than a fully model-based control strategy) to regulate the biogas production rate to a desired setpoint by manipulating the mixture ratio of the co-feedstocks in a real full-scale AcoD plant fed with corn silage, cattle manure, and other minor TS-rich agro-residues.

Mauky *et al.* [48] was the first work that considered (N)MPC of AcoD with an experimental validation carried out over a noteworthy 180 m^3 agro-industrial digester. The model complexity was stated to represent a good compromise considering the prediction accuracy, but under the very strong hypothesis of uninhibited operations only. Indeed, another similar experiment carried out in Körber *et al.* [41] highlighted the capability of a very simple model to suggest a dynamic feeding regime to match a desired biogas production, but this did not prevent the controller to temporarily overload the system reaching risky operative conditions in terms of VFAs accumulation. The main goal of these contributions was the track of a demand-driven production, rather than production optimization, making their approach unsuitable for the control problem of interest in this work. With the same goal of demand-driven production, Yoshida *et al.* [75] tested the tracking of a trapezoidal profile manipulating the overall OLR of a pilot-scale AcoD reactor fed with food and paper wastes: similar considerations can be derived, since a single-step linearized state-space data-driven model was employed (no need for state estimation, but recursive parameter update incorporated in the control scheme). Considering the possibility of dynamic diets and loading conditions, García-Gen *et al.* [27] combined linear programming and an ADM1-based AcoD model in an open-loop optimal control problem aimed at calculating the discrete-time evolution of the OLR and diet composition: the ADM1-based AcoD model is used to estimate the future biomethane production rates, based on the proposed sequence of future AcoD feedings optimized statically by the linear program. The OLR sequence is thus optimized dynamically by minimizing the biomethane flow rate tracking error. After a comprehensive modeling effort, Li *et al.* [44] exploited a linearized version of the ADM1 as predictor in an MPC to control a real lab-scale reactor: yet, the control problem was not extensively described and, to the authors' understanding, the controller was operated in an open-loop fashion, with the main goal of validating the predictive ability of the model. Bai *et al.* [10] studied fed-batch, small lab-scale AcoD of food and paper waste mixed with sieved cattle slurry, identifying a linear data-driven model and employing a Kalman Filter for state estimation. The control objective was the regulation of the biogas flow rate to a setpoint; however, the 21–day experimental campaign reported relatively limited tracking. Other valuable simulation studies of the advanced control of AcoD systems were conducted, but always missing the experimental validation [35], [74].

When looking for explicitly robust NMPC formulations applied to the AD process, the only contributions present in literature are 3 simulation-only works: one multi-scenario [55], one tube-based [16] (interestingly, both report the same way to assess the robustness of the controller with respect to the model uncertainties in the kinetic parameter values, i.e. MC

analysis [49]) and one multi-stage [35] (to handle the uncertainty in the characterization of the influent diet).

II. Materials and Methods

A. High-fidelity model: the agri-AcoDM model

The original ADM1 as implemented in Rosén&Jeppsson [61] was extended from its original purpose (the AD of waste sludge) to embrace the AcoD of multiple agro-industrial feedstocks. The resulting model was called "agri-AcoDM". The digester is represented as a 0-D CSTR, where the bulk liquid phase is treated as a three-phase heterogeneous mixture (soluble components, particulate matter, and dissolved gases), and the headspace gas phase is modeled as an ideal mixture of perfect gases. A description of each state variable is reported in Table S2. Details about the quantities involved in the fractionating of feedstocks' complex VS are reported in Section II-C. The main modifications and extensions are summarized hereafter:

- for each state variable, the influent forcing term is computed as the flow-weighted average of the corresponding influent concentrations in the co-feedstocks (ideal mixing, see for example Eq. (23));
- the disintegration process was neglected, as suggested by Batstone *et al.* [12] (original complex particulate variable X_C initialized in 0 and lack of any forcing term);
- the elemental composition of macromolecules X_{ch}, X_{pr}, X_{li} and microbial biomass was taken from Weinrich *et al.* [70];
- the unique state variables of biodegradable carbohydrates and proteins were de-lumped into three (readily $X_{ch,r}$, mildly $X_{ch,m}$, slowly $X_{ch,s}$) and two (readily $X_{pr,r}$, slowly $X_{pr,s}$) fractions with different hydrolytic behavior (first-order processes), similarly to Waskielis *et al.* [68];
- as it presents a different elemental composition with respect to the above-mentioned carbohydrates and particulate inerts X_I, a new inert state variable X_{lig} was added for lignin (composition taken from Triolo *et al.* [67]);
- for the same reason, another inert state variable X_p was added for dead microbial biomass, as suggested in Wett *et al.* [72] (N content taken from Koch *et al.* [40], C and P from Flores-Alsina *et al.* [21]);
- in time-varying AcoD operations, the elemental compositions of X_I and S_I (and the consequent COD over VS ratios) were computed dynamically depending on the mass apportion of inert macromolecules by the different co-feedstocks, to guarantee COD, C, N and P conservation across the digester;
- microbial biomass decay products were re-allocated into $X_{ch,s}$ (27.5%), $X_{pr,s}$ (27.5%), X_{li} (35%), X_I (8%, as in Koch *et al.* [40]) and S_I (remaining 2%);
- for a more accurate prediction of dissolved inorganic nutrients' availability and pH:
  - P was included as limiting nutrient in microbial kinetics, as in Flores-Alsina *et al.* [21], with the introduction of the S_{IP} state as a source-sink (biological assimilation/release) that guarantees elemental balance across the digester;
  - three liquid phase inorganic carbon species (dissolved carbon dioxide S_{co2}, bicarbonate S_{hco3}, and carbonate S_{co3}) and four inorganic phosphorus species (phosphate S_{po4}, hydrogen phosphate S_{hpo4}, dihydrogen phosphate S_{h2po4}, and phosphoric acid S_{h3po4}) were included. Furthermore, three cationic total components were added as states (potassium S_K, calcium S_{ca}, and magnesium S_{mg});
  - ionic strength I and consequent activity corrections were computed to account for the non-ideality of the acid-base equilibrium in the liquid bulk;
  - mineral precipitation was implemented as in Flores-Alsina *et al.* [21] and dissolution as in Aparicio *et al.* [6]. Four salts were selected and added as states, namely: amorphous calcium phosphate $Ca_3(PO_4)_2$ (X_{acp}), magnesium struvite $MgNH_4PO_4$ (X_{stru}), calcium carbonate $CaCO_3$ (X_{ccm}) and magnesite $MgCO_3$ (X_{mag});
- Monod functions were substituted with Haldane ones for total acetate (S_{ac}) and propionate concentration (S_{pro}) uptake by the acetate and propionate degraders (X_{ac} and X_{pro}) respectively;
- Temperature correction coefficients for mesophilic conditions were assumed as in Siegrist *et al.* [65].

Minor additional extensions include: (i) variable-volume operational mode; (ii) free ammonia gas/liquid mass transfer with the addition of the S_{gas,NH_3} state; (iii) correction of mass transfer coefficient (k_La) for different gases using their diffusivities.

Further details about the main model extensions are reported in Carecci *et al.* [14].

Figure S1 schematizes the main biomass transformation processes included in the model, mainly hydrolysis, acidogenesis, acetogenesis, acetoclastic and hydrogenotrophic methanogenesis, mineral precipitation and gas-liquid mass transfer.

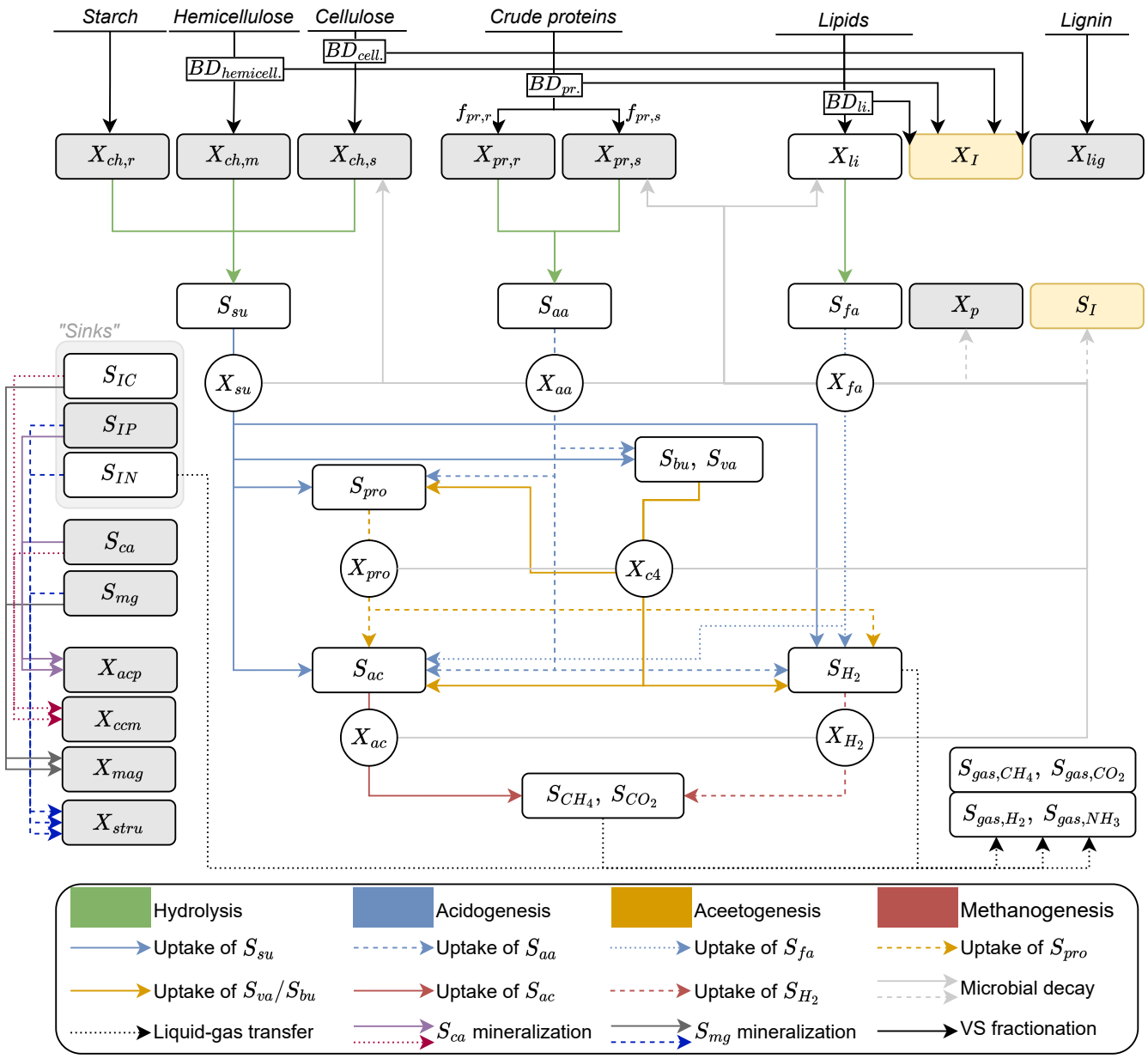

Fig. S1: Scheme of the AcoD process with reference to the agri-AcoDM model's state variables. Gray-colored boxes: new state variables; yellow-colored boxes: old states with modified elemental composition.

The original ADM1 was implemented in its differential algebraic equation (DAE) version, to reduce stiffness. However, the inclusion of precipitation processes (dynamics in the order of minutes) reintroduced a certain degree of stiffness, albeit to a lesser extent. The overall resulting DAE system is defined as Eq. (1), where $\mathbf{x} \in \mathbb{R}^n$ are dynamic state variables (mainly concentrations of chemical compounds and bacteria populations), $\boldsymbol{\psi}$ are algebraic variables (mainly physico-chemical quantities such as pH and I), $\mathbf{u} \in \mathbb{R}^m$ are inputs (the flow rates of the m co-feedstocks), $\boldsymbol{\theta}$ are uncertain parameters (both influent characteristics' matrix $\boldsymbol{\theta_{in}}$ with $\boldsymbol{\theta}_{\boldsymbol{in},i}$ columns $\forall i \in \{1,\dots,m\}$, and process $\boldsymbol{\theta_P}$) and $\mathbf{y}$ are measurable outputs. Functions $\mathbf{F}$ and $\mathbf{G}$ are non-linear (and in some cases not smoothly differentiable).

$$\begin{cases} \dot{\mathbf{x}} = \mathbf{F}(\mathbf{x}, \boldsymbol{\psi}, \mathbf{u}, \boldsymbol{\theta}) \\ \mathbf{0} = \mathbf{G}(\mathbf{x}, \boldsymbol{\psi}, \mathbf{u}, \boldsymbol{\theta}) \\ \mathbf{y} = \mathbf{H}(\mathbf{x}, \boldsymbol{\psi}, \mathbf{u}, \boldsymbol{\theta}) \end{cases} \tag{1}$$

The $\mathbf{F}$ mapping (the ODEs of the DAE system) system has the general form of Equation (2), where $\mathbf{x_{in}}$ represents influent concentrations, $D = \mathrm{HRT}^{-1}$ (d^{-1}) is the dilution rate, $\mathbf{K_G}$ is the stoichiometric (Gujer) matrix, $\mathbf{r_{bk}}(\mathbf{x})$ is the vector of biological reaction rates and $\mathbf{r_{pc}}(\mathbf{x})$ accounts for physicochemical processes (e.g. gas–liquid mass transfer).

$$\frac{d\mathbf{x}}{dt} = D \cdot (\mathbf{x_{in}} - \mathbf{x}) + \mathbf{K_G} \cdot \mathbf{r_{bk}}(\mathbf{x}) - \mathbf{r_{pc}}(\mathbf{x}) \tag{2}$$

The convective input term emphasizes the central role of feeding conditions: influent composition and loading directly affect reactor dynamics and, consequently, process stability (see Section II-C for further details). For simplicity, reactor volume loss due to biogas production is neglected and (digestate effluent flow rate = $\sum_{i=1}^{m} u_i$), although this assumption may introduce an error of approximately 5%. The main source of nonlinearities come in $\mathbf{r_{bk}}(\mathbf{x})$ and $\mathbf{r_{pc}}(\mathbf{x})$ mainly from the interconnected presence of acid-base equilibrium, pH computation (logarithmic expression), precipitation processes (nonlinear solubility products and exponential) and Monod/Haldane-like expressions of the microbial kinetics (see Eq. (25)). In particular, the Haldane function is non-monotonic function with uncertain shape that is commonly used to describe the link biomethane production and VFAs (e.g., S_{ac}) concentration via microbial' growth (e.g., X_{ac}), distinguishing *limited* from *inhibited* operating regions.

The values and descriptions of uncertain parameters and constants are reported in the original ADM1 manuscript and Carecci *et al.* [14], with the exception of the parameter subset that was tuned on data after model formalization, that are reported in Carecci *et al.* [17].

TABLE S2: Agri-AcoDM's initial conditions (at 13/04/2025 10AM) used to simulate the trajectories reported in the main manuscript (and in Figure S3 and S4), for reproducibility purposes.

Symbol (unit)	Value	Description
S_{aa} (g_{COD} L^{-1})	$4.398e^{-3}$	Soluble amino acids concentration in digestate
S_{ac} (g_{COD} L^{-1})	1.199	Acetic acid concentration in digestate
S_{an} (mmol L^{-1})	$2.266e^{-2}$	Residual anions concentration in digestate
S_{bu} (g_{COD} L^{-1})	$1.022e^{-2}$	Butyric acid concentration in digestate
S_{ca} (mmol L^{-1})	$8.627e^{-5}$	Total calcium concentration in digestate
S_{cat} (mmol L^{-1})	$8.530e^{-2}$	Residual cations concentration in digestate
S_{CH_4} (g_{COD} L^{-1})	$1.185e^{-1}$	Soluble methane concentration in digestate
S_{fa} (g_{COD} L^{-1})	$6.506e^{-2}$	Soluble long chain fatty acids (LCFA) concentration in digestate
$S_{gas,ch4}$ (g_{COD} L^{-1})	1.327	Methane concentration in biogas
$S_{gas,co2}$ (mmol L^{-1})	$1.556e^{-2}$	Carbon dioxide concentration in biogas
S_{gas,H_2} (g_{COD} L^{-1})	$1.399e^{-5}$	Hydrogen concentration in biogas
$S_{gas,nh3}$ (mmol L^{-1})	$1.155e^{-6}$	Ammonia concentration in biogas
S_{H_2} (g_{COD} L^{-1})	$7.320e^{-7}$	Soluble hydrogen concentration in digestate
S_I (g_{COD} L^{-1})	$8.477e^{-2}$	Soluble inerts concentration in digestate
S_{IC} (mmol L^{-1})	$1.334e^{-1}$	Total soluble inorganic carbon concentration in digestate
S_{IN} (mmol L^{-1})	$8.156e^{-2}$	Total soluble inorganic nitrogen concentration in digestate
S_{IP} (mmol L^{-1})	$8.193e^{-4}$	Total soluble inorganic phosphorus concentration in digestate
S_K (mmol L^{-1})	0	Total potassium concentration in digestate
S_{mg} (mmol L^{-1})	$8.549e^{-4}$	Total magnesium concentration in digestate
S_{pro} (g_{COD} L^{-1})	$5.582e^{-2}$	Propionic acid concentration in digestate
S_{su} (g_{COD} L^{-1})	$1.023e^{-2}$	Soluble monosaccharides concentration in digestate
S_{va} (g_{COD} L^{-1})	$5.224e^{-3}$	Valeric acid concentration in digestate
X_{aa} (g_{COD} L^{-1})	$3.131e^{-1}$	Amino Acid-degrading organisms concentration in digestate
X_{ac} (g_{COD} L^{-1})	$8.550e^{-1}$	Acetate-degrading organisms concentration in digestate
X_{acp} (mmol L^{-1})	0	Amorphous calcium phosphate concentration in digestate
X_C (g_{COD} L^{-1})	0	Complex particulate concentration in digestate
X_{c4} (g_{COD} L^{-1})	$3.169e^{-1}$	C4-degrading organisms concentration in digestate
X_{ccm} (mmol L^{-1})	$4.732e^{-3}$	Calcium carbonate concentration in digestate
$X_{ch,r}$ (g_{COD} L^{-1})	$4.591e^{-1}$	Particulate readily-biodegradable carbohydrates concentration in digestate
$X_{ch,m}$ (g_{COD} L^{-1})	$6.504e^{-1}$	Particulate mildly-biodegradable carbohydrates concentration in digestate
$X_{ch,s}$ (g_{COD} L^{-1})	2.825	Particulate slowly-biodegradable carbohydrates concentration in digestate
X_{fa} (g_{COD} L^{-1})	$2.512e^{-1}$	LCFA-degrading organisms concentration in digestate
X_{H_2} (g_{COD} L^{-1})	$4.573e^{-1}$	Hydrogen-degrading organisms concentration in digestate
X_I (g_{COD} L^{-1})	14.75	Particulate inerts concentration in digestate
X_{li} (g_{COD} L^{-1})	$7.659e^{-1}$	Particulate biodegradable lipids concentration in digestate
X_{lig} (g_{COD} L^{-1})	2.772	Lignin concentration in digestate
X_{mag} (mmol L^{-1})	$2.585e^{-7}$	Magnesite concentration in digestate
X_p (g_{COD} L^{-1})	$3.391e^{-1}$	Concentration in digestate of particulate inerts from bacteria decay
$X_{pr,r}$ (g_{COD} L^{-1})	$1.081e^{-1}$	Particulate readily-biodegradable proteins concentration in digestate
$X_{pr,s}$ (g_{COD} L^{-1})	$5.554e^{-1}$	Particulate slowly-biodegradable proteins concentration in digestate
X_{pro} (g_{COD} L^{-1})	$2.382e^{-1}$	Propionate-degrading organisms concentration in digestate
X_{stru} (mmol L^{-1})	$8.403e^{-3}$	Struvite concentration in digestate
X_{su} (g_{COD} L^{-1})	1.856	Monosaccharide-degrading organisms concentration in digestate
ash (g L^{-1})	13.09	Ash concentration in digestate

B. Reduced-order model(s)

Starting from the original AM2HN model of Hassam *et al.* [32], the AM2HN$_{tan}$ was formalized as a good trade-off to mimic ADM1-like behavior with reduced complexity.

With respect to the DAE system of the agri-AcoDM, the reduced-order models general formulation boils down to a simpler ODE, since there is not anymore any AE loop to be solved at each step for pH computation (see [11], [14] for further details). The system is defined in compact form by Eq. (3), where $\mathbf{f}$ and $\mathbf{h}$ are non-linear functions.

$$\begin{cases} \dot{\mathbf{x}} = \mathbf{f}(\mathbf{x}, \mathbf{u}, \boldsymbol{\theta}) \\ \mathbf{y} = \mathbf{h}(\mathbf{x}, \mathbf{u}, \boldsymbol{\theta}) \end{cases} \tag{3}$$

The vector state $\mathbf{x} \in \mathbb{R}^{n=m+7} = \{\mathbf{X_h}, X_1, X_2, S_1, S_2, Z, C, N\}$ contains:

- $\mathbf{X_h} \in \mathbb{R}^m$ (g_{VS} L^{-1}), that describes the hydrolysis of the biodegradable particulate VS fraction of each co-feedstock;
- X_1 and X_2 (g_{VS} L^{-1}), that describe the concentrations of acidogenic and methanogenic microbial biomass respectively, through substrate uptake and biomass decay;
- S_1 (g_{COD} L^{-1}) and S_2 (mmol L^{-1}), that describe the concentration of the biodegradable soluble COD and TVFA respectively, through hydrolysis and microbial metabolism/conversion;
- total alkalinity (i.e. TAC) concentration Z (mmol L^{-1}), impacted by N release from the hydrolysis of proteins, N microbial uptake and decay;
- inorganic dissolved carbon concentration C (mmol L^{-1}), produced via both acidogenesis and methanogenesis microbial metabolism/conversion and removed via liquid-gas CO_2 stripping;
- total ammonia nitrogen (i.e. TAN) concentration N (mmol L^{-1}), impacted by N release from the hydrolysis of proteins, N microbial uptake and decay.

With respect to the well-known AM2-core (X_1, X_2, S_1, S_2), the model incorporates both Z and C states as in the original full AM2 model to simulate pH and q_C (and, for the latter, exploit its measurement). As in the original AM2HN version, due to the low D typical of the operations of agro-industrial AcoD digesters, microbial decay and inorganic N release in Z were considered too. With respect to the original AM2HN model version, the $\mathbf{X_h}$ was extended from a single state variable to a vector $\in \mathbb{R}^m$, and the N state was added. Methanogens' inhibition by free ammonia concentration (S_{nh3} (mmol L^{-1})) was also added and modeled as a multiplicative non-competitive inhibition function in the methanogens' growth rate (μ_2) expression, following the common literature approach.

By applying mass balances to the state variables over the CSTR, considering the above-mentioned biochemical and physico-chemical processes affecting their dynamics, the ODE system described by Eq.s (4)–(11) is obtained:

$$\dot{\mathbf{X}}_\mathbf{h} = D(\mathbf{X_{h,in}} - \alpha \mathbf{X_h}) - \mathbf{k_h} \odot \mathbf{X_h} \tag{4}$$

$$\dot{X}_1 = (\mu_1 - \alpha D - k_{d,1}) X_1 \tag{5}$$

$$\dot{X}_2 = (\mu_2 - \alpha D - k_{d,2}) X_2 \tag{6}$$

$$\dot{S}_1 = D(S_{1,in} - S_1) - k_1 \mu_1 X_1 + \sum_{i=1}^{m} (COD_{X_h}/VS_{X_h})_i k_{h,i} X_{h,i} \tag{7}$$

$$\dot{S}_2 = D(S_{2,in} - S_2) + k_2 \mu_1 X_1 - k_3 \mu_2 X_2 \tag{8}$$

$$\dot{Z} = D(Z_{in} - Z) + \sum_{i=1}^{m} N_{X_{h,i}} k_{h,i} X_{h,i} - N_x[(\mu_1 - k_{d,1}) X_1 + (\mu_2 - k_{d,2}) X_2] \tag{9}$$

$$\dot{C} = D(C_{in} - C) + k_4 \mu_1 X_1 + k_5 \mu_2 X_2 - q_C \tag{10}$$

$$\dot{N} = D(N_{in} - N) + \sum_{i=1}^{m} N_{X_{h,i}} k_{h,i} X_{h,i} - N_x[(\mu_1 - k_{d,1}) X_1 + (\mu_2 - k_{d,2}) X_2] \tag{11}$$

$$y_1 = q_M = k_6 \mu_2 X_2 \tag{12}$$

$$y_2 = q_C = k_L a (CO_2 - k_H P_c) \tag{13}$$

where:

$$D = \frac{\sum_{i=1}^{m} u_i}{V} \tag{14}$$

$$\mu_1 = \mu_{max,1} \frac{S_1}{S_1 + K_{S,1}} \tag{15}$$

$$\mu_2 = \mu_{max,2} \frac{S_2}{S_2 + K_{S,2} + \frac{S_2^2}{K_{I,2}}} \left(\frac{K_{I,nh3}}{K_{I,nh3} + S_{nh3}} \right) \tag{16}$$

$$CO_2 = C + S_2 - Z \tag{17}$$

$$\phi = CO_2 + k_H P_{tot} + \frac{q_M}{k_L a} \tag{18}$$

$$Pc = \frac{\phi - \sqrt{\phi^2 - 4 k_H P_{tot} CO_2}}{2 k_H} \tag{19}$$

$$pH = -\log_{10} \left(\frac{K_{a,co2} CO_2}{Z - S_2} \right) \tag{20}$$

$$S_H^+ = \left(\frac{1}{10} \right)^{pH} \tag{21}$$

$$S_{nh3} = \frac{K_{a,nh4} N}{K_{a,nh4} + S_H^+} \tag{22}$$

$$x_{in}^{(j)} = \frac{\sum_{i=1}^{m} u_i \theta_{in,i}^{(j)}}{\sum_{i=1}^{m} u_i}, \qquad j \in \{S_1, S_2, Z, C, N\} \tag{23}$$

$$\mathbf{X_{h,in}} = \frac{\mathbf{u} \odot \mathbf{BD_{VS_p}} \odot \mathbf{VS_p}}{\sum_{i=1}^{m} u_i} \tag{24}$$

The inputs $\mathbf{u} \in \mathbb{R}^m$ are the flow rates of the co-feedstocks (L d^{-1}) and, for consistency with the industrial practice, the *online* outputs $\mathbf{y} \in \mathbb{R}^2 = \{q_M, q_C\}$ are only the biomethane (q_M) and carbon dioxide (q_C) flow rates (mmol L^{-1} d^{-1}). V (L) is the reactor liquid working volume and D (d^{-1}) is the dilution rate (inverse of HRT). The presence of multiplicative Monod, Haldane and/or non-competitive inhibition functions in the expression of the kinetic growth rates of microbes (Eq.s (15)–(16)) builds up the non-linearity of the model. Indeed, a Haldane-like function (μ_2 (d^{-1}), Eq. (16)) is used in the description of q_M production from the uptake of TVFA (state S_2 (mmol L^{-1})) by methanogens (state X_2 (g L^{-1})). Note that the shape parameters of such non-monotonic function are uncertain and distinguish a *limited* from an *inhibited* operating region. P_c (bar) stands for the partial pressure of CO_2 in the gaseous head-space of the reactor and it is used in the q_C computation. The biodegradability ($\mathbf{BD_{VS_p}}$) of the particulate fraction of the volatile solids ($\mathbf{VS_p}$) of each co-feedstock is a vector with m entries fixed as constants and computed from the chemical and biochemical characterizations [14]. Same holds for the N concentrations ($\mathbf{N_{X_h}}$) and the COD over VS ratios ($\mathbf{COD_{X_h}/VS_{X_h}}$) of $\mathbf{X_h}$. Similarly, each entry of $\boldsymbol{\theta_{in,i}}$ is set from feedstocks' characterization, but it can be time-varying and its flow-weighted average is used to compute the corresponding entry of the reactor's influent forcing term vector $\mathbf{x_{in}}$ (Eq. (23)). See Section II-C for further details. The values of other constants such as the microbial biomass N content (N_x) and the physico-chemical equilibrium constants were taken from the original ADM1 values (corrected with the actual process temperature T). Unit density for the solid-liquid organic mixtures (feedstocks and digestate) was considered. The parameter α (i.e. the ratio between the particulate and soluble matter retention times) was set to unity. The values and descriptions of uncertain parameters and constants are reported in Tables S3 and S4 respectively.

In this work, considering that the system under investigation is highly buffered (N and pH dynamics are dampened) and that the feeding rates of N-rich co-feedstocks were not used as control actions, ammonia inhibition was neglected and a simpler AM2HN version was derived by:

- removing Eq. (11) (the N state equation);
- reducing the μ_2 expression to the sole original Haldane function for VFA (from Eq. (16) to Eq. (25)).

$$\mu_2 = \mu_{max,2} \frac{S_2}{S_2 + K_{S,2} + \frac{S_2^2}{K_{I,2}}} \tag{25}$$

In other words, compared to the slightly more comprehensive AM2HN$_{tan}$ model, the almost-constant inhibition effect was indirectly considered in the training phase by the estimation of lower/higher values of the methanogens' maximum growth rate ($\mu_{max,2}$)/ half-saturation ($K_{S,2}$) constants, respectively.

The reduced-order model was tuned in Carecci *et al.* [17] following a double-stage estimation: first, all parameters were estimated minimizing the simulation error with respect to a highly-informative synthetic dataset generated from the agri-AcoDM under strongly exciting and well-distributed inputs' profiles ("physically-informed" training). Later, a refinement on real data of the practically identifiable parameters $\boldsymbol{\theta_{PSS}} \subset \boldsymbol{\theta_P}$ (parameter subset selection (PSS) algorithm based on sensitivity and Fisher Information Matrix (**FIM**) computations) was carried out [17].

Moreover, following structural observability analysis (unobservability of both C and Z) and practical considerations for real-time implementation (presence of a gasbag before actual biogas composition measurement), some additional modifications to the above-mentioned AM2HN model version were made:

- a new state variable ξ (mmol L^{-1}) was introduced and defined as the difference between Z and C: Eq.s (9)–(10) were substituted with Eq. (26). As a consequence, the dissolved CO_2 concentration expressed by Eq. (17) was substituted with Eq. (27);

$$\dot{\xi} = \dot{Z} - \dot{C} = D(\xi_{in} - \xi) + \sum_{i=1}^{m} N_{X_{h,i}} k_{h,i} X_{h,i} - N_x[(\mu_1 - k_{d,1})X_1 + (\mu_2 - k_{d,2})X_2] - k_4\mu_1 X_1 - k_5\mu_2 X_2 + q_C \tag{26}$$

$$CO_2 = S_2 - \xi \tag{27}$$

- a new state variable $x_{M,gb}$ (-) was introduced to model the fraction of biomethane at the outlet of a biogas gasbag present between the CSTR and the gas analyzer. Its expression was derived from the molar balance across the gasbag volume (V_{gb} (L)), and, as a result, Eq. (28) was added to the ODE system. Accordingly, the biomethane flow rate at the gasbag outlet is computed from Eq. (29).

$$\dot{x_{M,gb}} = \frac{VRT}{1 \times 10^3 V_{gb} P_{tot}} (q_M - (q_C + q_M) x_{M,gb}) \tag{28}$$

$$q_{M,gb} = x_{M,gb} q_{TOT} \tag{29}$$

The resulting final and locally structurally observable control-oriented model that was used for state estimation and model-based control was obtained, hereafter referred to as the "AM2HN$_{obs}$" model. In the latter, the vector state is $\mathbf{x} \in \mathbb{R}^{n=m+6} = \{\mathbf{X_h}, X_1, X_2, S_1, S_2, \xi, x_{M,gb}\}$.

The *online* outputs $\mathbf{y} \in \mathbb{R}^3 = \{q_{TOT}, x_{M,gb}, x_{C,gb}\}$ are the biogas flow rate (mmol L^{-1} d^{-1}) and its composition in terms of CH_4 ($x_{M,gb}$) and CO_2 ($x_{C,gb}$) fractions, where $q_{TOT} = q_C + q_M$ and $x_{C,gb} = 1 - x_{M,gb}$. The biogas composition fractions were chosen as outputs rather than the corresponding flow rates to mitigate noise amplification and thus improve state estimation. This selection ensures greater consistency with the raw measurements, minimizing error propagation due to additional signal processing, and accounts for the higher noise levels typically affecting biogas flow rate data compared to gas composition measurements (see the **R** values reported in the main manuscript).

The initialization of the state vector used in the present work is reported in Table S5.

TABLE S3: AM2HN$_{obs}$' parameter values (see [17] for further details). Parameters that belong to $\boldsymbol{\theta_{PSS}}$ are recognizable by the values for which non-negligible ± 95% confidence intervals were reported.

Symbol (unit)	Value*	Description
α (-)	1	Fraction of microbial biomass in the liquid phase (process heterogeneity)
k_1 (g_{COD} g_{VS}^{-1})	14.5	Stoichiometric coefficient for S_1 consumption during acidogenesis
k_2 (mmol g_{VS}^{-1})	154	Stoichiometric coefficient for S_2 production during acidogenesis
k_3 (mmol g_{VS}^{-1})	335	Stoichiometric coefficient for S_2 consumption during methanogenesis
k_4 ($mmol_C$ g_{VS}^{-1})	34.5	Stoichiometric coefficient for CO_2 production during acidogenesis
k_5 ($mmol_C$ g_{VS}^{-1})	391 ± 2	Stoichiometric coefficient for CO_2 production during methanogenesis
k_6 ($mmol_C$ g_{VS}^{-1})	485 ± 2	Stoichiometric coefficient for CH_4 production during methanogenesis
k_La (d^{-1})	30**	Gas–liquid mass transfer coefficient
$K_{I,2}$ (mmol L^{-1})	55.3	TVFA inhibition constant of methanogens
$K_{S,1}$ (g_{COD} L^{-1})	6.4	Half-saturation constant for acidogenic biomass growth
$K_{S,2}$ (mmol L^{-1})	27.7 ± 0.6	Half-saturation constant for methanogenic biomass growth
$\mu_{max,1}$ (d^{-1})	8.1	Maximum specific growth rate of acidogens
$\mu_{max,2}$ (d^{-1})	0.14	Maximum specific growth rate of methanogens
$k_{d,1}$ (d^{-1})	0.032	Decay rate of acidogens
$k_{d,2}$ (d^{-1})	0.011	Decay rate of methanogens
$\mathbf{k_h}$ ($\mathbf{d^{-1}}$)	[0.22 ± 0.01, 0.14 ± 0.02, 0.48 ± 0.13]	Hydrolysis constants
$K_{I,nh3}$*** ($mmol_N$ L^{-1})	8.7	Free ammonia inhibition constant of methanogens

**taken from Carecci et al. [17].*
***manually re-tuned in this work, starting from literature correlations [39]*
****used only in the AM2HN$_{tan}$ model version. See Carecci et al. [17] for AM2HN$_{tan}$-coherent parametrization.*
S_2 value at the Haldane μ_2 peak at 39.2 mmol L^{-1}.

TABLE S4: AM2HN$_{obs}$' constants.

Symbol (unit)	Value	Description
V (L)	12	Reactor liquid working volume
V_{gb} (L)	4.5	Gasbag volume
T (°C)	42	Operating temperature
N_x (mmol$_N$ g$_{VS}^{-1}$)	8.58	Nitrogen content in microbial biomass
$\mathbf{COD_{X_h}/VS_{X_h}}$ ($\mathbf{g_{COD}g_{VS}^{-1}}$)	[1.27, 1.49, 1.74]	COD over VS ratio of the particulate biodegradable fraction of VS
$\mathbf{N_{X_h}}$ ($\mathbf{mmol_N g_{VS}^{-1}}$)	[0.89, 1.53, 7.69]	Nitrogen content of the particulate biodegradable fraction of VS
k_H (mmol L^{-1} bar^{-1})	22.7	Henry's constant for CO_2
P_{tot} (bar)	1.035	Total pressure in the CSTR gaseous headspace
$K_{a,co2}$ (mmol L^{-1})	5.08e^{-7}	First dissociation constant of the CO_2/HCO_3^- system
$K_{a,nh4}$* (mmol L^{-1})	1.85e^{-9}	Dissociation constant of the NH_4^+/NH_3 equilibrium

**used only in the AM2HN$_{tan}$ model version.*

TABLE S5: AM2HN$_{obs}$' initial conditions (at 13/04/2025 10AM), and $\mathbb{Z}$ and $\mathbb{X}$ bounds. For vectors $\in \mathbb{R}^m$ it holds: (1): maize silage, (2): cow slurry, (3): tomato sauce.

	$\hat{\mathbf{x}}_0$	$\mathbf{z_{lb}}$, $\mathbf{z_{ub}}$	$\mathbf{x_{lb}}$, $\mathbf{x_{ub}}$
$X_h^{(1)}$ (gVS L^{-1})	2.91	2.00e^{-6}, 15.0	2.00e^{-6}, 15.0
$X_h^{(2)}$ (gVS L^{-1})	1.20	2.00e^{-6}, 15.0	2.00e^{-6}, 15.0
$X_h^{(3)}$ (gVS L^{-1})	2.10e^{-1}	2.00e^{-6}, 1.00	2.00e^{-6}, 10.0
X_1 (gVS L^{-1})	1.53	2.00e^{-6}, 3.00	2.00e^{-6}, 10.0
X_2 (gVS L^{-1})	1.26	1.00, 6.00	2.00e^{-6}, 10.0
S_1 (g$_{COD}$ L^{-1})	8.36e^{-2}	2.00e^{-6}, 3.00e^{-1}	2.00e^{-6}, 1.00
S_2 (mmol L^{-1})	18.8	1.00, 15.0	2.00e^{-6}, 60.0
ξ (mmol L^{-1})	8.32	-30.0, 10.0	-35.0, 35.0
$x_{M,gb}$ (-)	5.70e^{-1}	5.00e^{-1}, 9.00e^{-1}	3.50e^{-1}, 9.00e^{-1}

C. Co-feedstocks' characterization

A good characterization for each co-feedstock is usually available in full-scale plants, yet with infrequent updates (e.g. seasonal) to follow, coherently, the most relevant variations (e.g. $\approx$ 10% difference in the maize silage VS concentration over 6 months of trench storage). As a result, where possible, the values in Table S6 were taken from measurements conducted for this work and data provided by the feedstock's suppliers.

To emulate the input variability typical of full-scale operations, fresh batches of maize silage and cattle slurry were collected from the same nearby dairy farm every 3 to 4 weeks. Feedstock characterization was intentionally not updated at each batch change — as this would not be practically scalable — with the exception of TS and VS, in line with full-scale practice.

BMP tests were conducted in duplicate to measure the biodegradability (BD_{VS}) and BMP$_\infty$ of the feedstocks' overall VS. BMP data were also used to verify the consistency of the $\mathbf{k_h}$ (hydrolytic behavior approximated by first-order model) values considered in this work and previously estimated in Carecci *et al.* [17].

Where not available, literature values were hypothesized and manually adapted to match the measurements; this held for example for: (i) the concentration of calcium and magnesium cations in cow slurry and tomato sauce; (ii) the protein, lipid and carbohydrate content (and composition) of cow slurry; and (iii) the repartition of the BD_{VS} measured from BMP tests into proteins, lipids, cellulose and hemicellulose (adjusting manually to match the BMP$_\infty$). Then, for each co-feedstock: (i) VS_p was computed subtracting from VS all organic acids and simple sugars; (ii) BD_{VS_p} was computed weighting each particulate fraction by its biodegradability (100% and 0% biodegradability for starch and lignin respectively); (iii) N_{X_h} was computed from the N content of amino acids and biodegradable proteins; and (iv) COD_{X_h}/VS_{X_h} was computed weighing the biodegradable fraction of each VS_p contribution by their literature COD/VS ratio [21], [70]. Consequently, the total COD and related biodegradability (BD_{COD}) were computed. The theoretical BMP$_\infty$ (BMP$_{th}$) was computed considering 100% biodegradability for each macromolecule.

TABLE S6: Feedstocks' composition data (as measured/from literature).

	Maize silage*	**Cow slurry**	**Tomato sauce***	**Note**
TS (g_{TS} L^{-1})	364.4	39.00	94.51	Measured
VS (%TS)	93.39	70.60	85.40	Measured
pH (-)	4.00	7.44	4.73	Measured
TAC (mg_{CaCO_3} L^{-1})	0	7263.3	0	Measured
TAN (mgN L^{-1})	0	920.00	677.91	Measured
P-PO_4 (mg_P L^{-1})	0	88.50	260.0	Measured
Calcium (mol L^{-1})	$1.00e^{-2}$	$3.50e^{-3}$	$3.25e^{-3}$	Measured. From [14] for cow slurry.
Magnesium (mol L^{-1})	$1.97e^{-2}$	$7.00e^{-3}$	$6.58e^{-3}$	Measured. From [14] for cow slurry.
Acetate (g_{COD} L^{-1})	8.870	1.970	1.257	Measured
Propionate (g_{COD} L^{-1})	2.538	1.210	0	Measured
Butyrate (g_{COD} L^{-1})	0	$3.341e^{-1}$	0	Measured
Valerate (g_{COD} L^{-1})	0	$2.996e^{-1}$	$1.510e^{-1}$	Measured
Sugar (%TS)	6.582	0	52.55	From supplier data
Amino-acid (%TS)	0	0	0	From supplier data
Long-ch. VFA (%TS)	0	0	0	From supplier data
BMP_∞ (NmL_{CH_4} g_{VS}^{-1})	421	202	386	Measured
Protein (%TS)	6.533	13.27	18.68	From supplier data. From [14] for cow slurry.
Lipid (%TS)	3.826	4.160	5.839	From supplier data. From [14] for cow slurry.
Cellulose (%TS)	16.49	14.29	0	From supplier data. From [14] for cow slurry.
Hemicell. (%TS)	15.23	8.713	7.007	From supplier data. From [14] for cow slurry.
Lignin (%TS)	4.148	11.70	0	From supplier data. From [14] for cow slurry.
Starch (%TS)	38.15	10.60	0	From supplier data. From [14] for cow slurry.
$BD_{protein}$ (%)	77	25	50	Taken from [69] and manually adjusted
BD_{lipids} (%)	100	100	50	Taken from [69] and manually adjusted
$BD_{cellulose}$ (%)	36	35	0	Taken from [30], [47], [63] and manually adjusted
$BD_{hemicell.}$ (%)	95	35	35	Taken from [30], [63] and manually adjusted
Carbohyd. (%TS)	80.59	45.29	59.55	Computed
BD_{VS} (%)	82.15	47.79	80.30	Computed
BMP_{th} (NmL_{CH_4} g_{VS}^{-1})	448.5	485.2	456.6	Computed
Tot. COD (g_{COD} L^{-1})	436.1	38.15	105.3	Computed
BD_{COD} (%)	82.12	49.98	74.78	Computed
VS_p (g_{VS_p} L^{-1})	316.4	27.52	31.04	Computed
BD_{VS_p} (%)	77.65	36.99	44.79	Computed

**exclude VFAs in VS as in Weissbach et al. [71].*

The values in Table S6 are supplied to the agri-AcoDM Modelica model, and they are converted to the values in Table S7 (each column is $\boldsymbol{\theta}_{\mathbf{in},i}$ for $i \in \{1,..,m\}$ with $m = 3$), i.e. in terms of state variables, to finally compute, by means of weighted average over the different co-feedstock's input flow rates, the $\mathbf{x_{in}}$. In this work it was assumed that null soluble inerts (S_I) are present in all feedstock: although this does not reflect reality, especially for cow slurry, such assumption is justified as the difference between particulate inerts (X_I) and S_I does not affect the results reported in the main manuscript. For simplicity, for the feedstocks of interest, soluble amino-acids and long-chain fatty acids were considered to be null, whereas the total particulate COD (net of organic acids and soluble simple sugars) was fractionated into readily $X_{ch,r}$ (starch), mildly $X_{ch,m}$ (hemicellulose) and slowly $X_{ch,s}$ (cellulose) biodegradable carbohydrates, readily $X_{pr,r}$ and slowly $X_{pr,s}$ biodegradable proteins (hypothesized to be both 50% (f_{pr}) of the total crude protein concentration) and lipids (X_{li}). Null active/dead microbial matter and precipitated salt concentrations were hypothesized for all co-feedstocks (although this may be imprecise especially for cow slurry). From the TAC, pH, VFAs and TAN data, the dissolved inorganic carbon S_{IC} concentration is computed; afterward, cations (S_{cat}) concentration is derived to close the charge neutrality equation (a fixed anions S_{an} concentration is hypothesized). The correspondence between the agri-AcoDM and AM2HN models' state variables, with the appropriate unit conversions, is reported in the Digital Supplementary Material of Carecci *et al.* [17].

The values in Table S8 were thus derived.

TABLE S7: Feedstocks' composition in terms of the agri-AcoDM model's state variables (i.e. $\boldsymbol{\theta_{in}}$ matrix).

	Maize silage	**Cow slurry**	**Tomato sauce**
S_{aa} (g_{COD} L^{-1})	0	0	0
S_{ac} (g_{COD} L^{-1})	8.870	1.970	1.257
S_{an} (mmol L^{-1})	0	$2.000e^{-2}$	$5.000e^{-2}$
S_{bu} (g_{COD} L^{-1})	0	$3.341e^{-1}$	0
S_{ca} (mmol L^{-1})	$1.000e^{-2}$	$3.500e^{-3}$	$3.250e^{-3}$
S_{cat} (mmol L^{-1})	0	$8.141e^{-2}$	$7.180e^{-5}$
S_{CH_4} (g_{COD} L^{-1})	0	0	0
S_{fa} (g_{COD} L^{-1})	0	0	0
S_{H_2} (g_{COD} L^{-1})	0	0	0
S_I (g_{COD} L^{-1})	0	0	0
S_{IC} (mmol L^{-1})	0	$1.057e^{-1}$	0
S_{IN} (mmol L^{-1})	0	$6.571e^{-2}$	$4.842e^{-2}$
S_{IP} (mmol L^{-1})	0	$2.857e^{-3}$	$8.394e^{-3}$
S_K (mmol L^{-1})	0	0	0
S_{mg} (mmol L^{-1})	$1.970e^{-2}$	$7.000e^{-3}$	$6.584e^{-3}$
S_{pro} (g_{COD} L^{-1})	2.538	1.210	0
S_{su} (g_{COD} L^{-1})	25.66	0	53.14
S_{va} (g_{COD} L^{-1})	0	$2.996e^{-1}$	$1.510e^{-1}$
X_{aa} (g_{COD} L^{-1})	0	0	0
X_{ac} (g_{COD} L^{-1})	0	0	0
X_{acp} (mmol L^{-1})	0	0	0
X_C (g_{COD} L^{-1})	0	0	0
X_{c4} (g_{COD} L^{-1})	0	0	0
X_{ccm} (mmol L^{-1})	0	0	0
$X_{ch,r}$ (g_{COD} L^{-1})	164.7	4.898	0
$X_{ch,m}$ (g_{COD} L^{-1})	62.47	1.410	2.747
$X_{ch,s}$ (g_{COD} L^{-1})	25.64	2.311	0
X_{fa} (g_{COD} L^{-1})	0	0	0
X_{H_2} (g_{COD} L^{-1})	0	0	0
X_I (g_{COD} L^{-1})	57.26	12.85	26.42
X_{li} (g_{COD} L^{-1})	39.47	4.593	7.810
X_{lig} (g_{COD} L^{-1})	20.58	6.211	0
X_{mag} (mmol L^{-1})	0	0	0
X_p (g_{COD} L^{-1})	0	0	0
$X_{pr,r}$ (g_{COD} L^{-1})	14.03	$9.897e^{-1}$	6.756
$X_{pr,s}$ (g_{COD} L^{-1})	14.03	$9.897e^{-1}$	6.756
X_{pro} (g_{COD} L^{-1})	0	0	0
X_{stru} (mmol L^{-1})	0	0	0
X_{su} (g_{COD} L^{-1})	0	0	0
ash (g L^{-1})	24.09	11.47	13.80

TABLE S8: Feedstocks' composition in terms of the AM2HN$_{tan}$ model's state variables (i.e. $\boldsymbol{\theta_{in}}$ matrix).

	Maize silage	**Cow slurry**	**Tomato sauce**
$X_h^{(1)}$ (g_{VS} L^{-1})	245.63	-	-
$X_h^{(2)}$ (g_{VS} L^{-1})	-	10.18	-
$X_h^{(3)}$ (g_{VS} L^{-1})	-	-	13.91
X_1 (g_{VS} L^{-1})	0	0	0
X_2 (g_{VS} L^{-1})	0	0	0
S_1 (g_{COD} L^{-1})	25.66	0	53.14
S_2 (mmol L^{-1})	161.26	45.11	20.36
Z (mmol L^{-1})	0	145.27	0
C (mmol L^{-1})	0	123.00	0
N (mmol L^{-1})	0	65.71	48.42

D. Analytical methods

The bench-scale reactors were mixed continuously with rotors set between 120–180 rpm.

BMP tests were conducted using an Automatic Methane Potential Test System (AMPTS II Light, Bioprocess Control AB, Sweden) comprising six glass reactors, each with a total volume of 2.3 L and a working volume of 2 L. These were incubated under constant mesophilic conditions (42 $\pm$ 1°C) and mixed intermittently, following a duty cycle of 5 min on and 15 min off, to maintain homogeneous sludge–substrate suspensions. The inoculum to substrate ratio was set to 2.5 (based on volatile solids). Blank bottles containing inoculum only were also included. Prior to use, the headspace of each reactor was flushed with N_2 gas. During operation, CO_2 was absorbed in an alkali trap (3 M sodium hydroxide solution with a 0.4% thymolphthalein indicator) to ensure accurate CH_4 measurement. The AMPTS II Light system automatically recorded cumulative gas volumes and corrected for temperature and pressure, enabling the direct calculation of the specific biomethane yield. Incubation continued until biogas production from all reactors reached a plateau (termination criterion: net daily production over the last three days $< 1\%$).

The routine analysis of pH, TS, VS, COD and alkalinity was performed in accordance with Standard Methods [7]. pH was monitored using a benchtop pH meter (HI5521, Hanna Instruments Inc., USA) in accordance with Method 4500-H^+. TS and VS were determined according to Method 2540 using a drying oven (UF75, Memmert, Germany), a muffle furnace (FB1410M-33, Thermolyne, Thermo Scientific, USA) and an analytical balance (ENTRIS II BCE224i-1S, Sartorius, Germany). Total and soluble COD were measured using Method 5220.D, employing a digestion reactor (HI839800 COD Test Tube Heater, Hanna Instruments, USA) and a spectrophotometer (DR3900, Hach, USA). Samples for soluble COD quantification were previously centrifuged (DM0412, DLAB Scientific, China) and filtered through a 0.45 μm filter. TAC was measured by titration according to Method 2320. Additionally, partial alkalinity (PA) and IA were determined according to Ripley *et al.* [59]. PA was obtained via direct titration to a pH endpoint of 5.75, and IA was obtained from a pH of 5.75 to 4.3. TAN was determined using the HANNA Instruments Nessler method (an adapted version of the ASTM D1426 and Standard Methods 4500-NH_3 methods) [31], and absorbance was measured using a Hach DR3900 spectrophotometer.

VFAs (acetic, propionic, butyric, and valeric acids) were quantified using a custom analytical protocol based on gas chromatography with flame ionization detection (GC-FID), using a gas chromatograph (HP 5890 Series II, Hewlett-Packard, USA) equipped with a HP-1 capillary column (30 m $\times$ 0.53 mm $\times$ 0.2 μm). Hereafter the details about the procedure followed to quantify VFAs during the experimental campaign of interest for the current work:

Sample preparation: samples were first homogenized, and approximately 10 mL was transferred to a 15 mL centrifuge tube and centrifuged at 4000 rpm for 15 min. Aliquots of the clarified supernatant (1–2 mL) were distributed into eight 7 mL vials according to the standard-addition scheme. Each vial contained either 2 mL of sample and 1 mL of ultrapure water (vials 1–4) or 1 mL of sample and 2 mL of ultrapure water (vials 5–8). To all vials, 50 μL of an internal-standard stock solution (1-butanol, 50 μL $\cdot$ 5 mL^{-1} H_2O) was added. Known volumes of a VFA mixed stock solution (acetic, propionic, butyric, and valeric acids, 50 μL $\cdot$ 5 mL^{-1} H_2O) were then added as follows: 20 μL to vial 7, 30 μL to vial 3, and 60 μL to vials 4 and 8. All vials were capped, mixed thoroughly, and acidified with 100 μL of phosphoric acid. The mixtures were centrifuged at 1000 rpm for 10 min, and 1 μL of the clear supernatant was injected into the GC-FID. A separate 1 μL injection of the internal standard solution was also analyzed.

Chromatographic conditions: N_2 was used as the carrier gas at 5 psi, with a purge flow of 1 mL min^{-1} and a split flow of 50 mL min^{-1}. Injector and detector temperatures were set to 250°C and 290°C, respectively. For acetic acid determination, the oven temperature program was: 40°C (2 min), ramp at 5°C min^{-1} to 55°C (hold 0 min), then 40°C min^{-1} to 290°C. The injection mode was splitless (1 μL, 0.1 min). For propionic, butyric, and valeric acids, the program was: 40°C (2 min), ramp at 5°C min^{-1} to 60°C (0 min), then 10°C min^{-1} to 110°C (0 min), and finally 40°C min^{-1} to 290°C. The injection mode was splitless (1 μL, 0.3 min).

Quantification and data treatment: peak areas of each acid were corrected relative to the internal standard area in both the samples and the internal standard solution to account for injection variability and volumetric dilution. Quantification was based on standard-addition calibration curves constructed for each acid: acetic acid from vials 1–3–4 and 2–3–4, and propionic, butyric, and valeric acids from vials 5–7–8 and 6–7–8. Concentrations were expressed as mg L^{-1} of each acid in the original sample.

E. EKF formulation

The discretized version of Eq. (3), for each discrete time instant t of integration, is described by Eq. (30).

$$\begin{cases} \mathbf{x}_t = \mathbf{x}_{t-1} + \Delta t \cdot \mathbf{f}(\mathbf{x}_{t-1}, \mathbf{u}_{t-1}, \theta) = \mathbf{f}_\Delta(\mathbf{x}_{t-1}, \mathbf{u}_{t-1}, \theta) \\ \mathbf{y}_t = \mathbf{h}_\Delta(\mathbf{x}_t, \mathbf{u}_t, \theta) \end{cases} \tag{30}$$

Eq. (31) expresses the discrete system in its linearized form at t, where the $\mathbf{A}_t$ and $\mathbf{C}_t$ matrices are the time-varying Jacobians of $\mathbf{f}_\Delta$ and $\mathbf{h}_\Delta$ with respect to states, and $\mathbf{B}_t$ is the time-varying Jacobian of $\mathbf{f}_\Delta$ with respect to the inputs.

$$\begin{cases} \mathbf{x}_{t+1} = \mathbf{A}_t \mathbf{x}_t + \mathbf{B}_t \mathbf{u}_t \\ \mathbf{y}_t = \mathbf{C}_t \mathbf{x}_t \end{cases} \tag{31}$$

$$\mathbf{A}_t = \left.\frac{\partial \mathbf{f}_\Delta(\mathbf{x}_t, \mathbf{u}_t)}{\partial \mathbf{x}_t}\right|_{\mathbf{x}_t, \mathbf{u}_t}, \qquad \mathbf{B}_t = \left.\frac{\partial \mathbf{f}_\Delta(\mathbf{x}_t, \mathbf{u}_t)}{\partial \mathbf{u}_t}\right|_{\mathbf{x}_t, \mathbf{u}_t}, \qquad \mathbf{C}_t = \left.\frac{\partial \mathbf{h}_\Delta(\mathbf{x}_t, \mathbf{u}_t)}{\partial \mathbf{x}_t}\right|_{\mathbf{x}_t} \tag{32}$$

The discrete-time EKF is formalized based on the time discretization of Eq. (3) The model was discretized using a forward-Euler scheme with integration step Δ_t, and the EKF relies on linearization of the state-transition and observation equations (Jacobian matrices computed via finite differences).

Kalman filtering is based on the hypothesis of perfect knowledge of the real system, except for (known) Gaussian process and measurement noises: the real system is hypothesized to be described by Eq. (33), i.e. exactly equal to the open-loop model of Eq. (31) with the addition of the above-mentioned noises.

$$\begin{cases} \tilde{\mathbf{x}}_t = \mathbf{A}_{t-1} \tilde{\mathbf{x}}_{t-1} + \mathbf{B}_{t-1} \mathbf{u}_{t-1} + \mathbf{w}_{t-1} \\ \tilde{\mathbf{y}}_t = \mathbf{C}_t \tilde{\mathbf{x}}_t + \mathbf{v}_t \end{cases} \tag{33}$$

The process ($\mathbf{w}_t$) and measurement noises ($\mathbf{v}_t$) are white, zero-mean, uncorrelated, and have known covariance matrices $\mathbf{Q}$ and $\mathbf{R}$, respectively, that are the tuning parameters of the filter.

$$\mathbf{w}_t \sim \mathcal{N}(0, \mathbf{Q}) \tag{34}$$

$$\mathbf{v}_t \sim \mathcal{N}(0, \mathbf{R}) \tag{35}$$

$$\mathbf{A}_{t-1} = \left.\frac{\partial \mathbf{f}_\Delta(\mathbf{x}_{t-1}, \mathbf{u}_{t-1})}{\partial \mathbf{x}_{t-1}}\right|_{\mathbf{x}_{t-1} = \mathbf{x}_{t-1}^+} \tag{36}$$

$$\mathbf{C}_t = \left.\frac{\partial \mathbf{h}_\Delta(\mathbf{x}_t, \mathbf{u}_t)}{\partial \mathbf{x}_t}\right|_{\mathbf{x}_t = \mathbf{x}_t^-} \tag{37}$$

Since $\mathbf{A}_{t-1}$, $\mathbf{B}_{t-1}$ and $\mathbf{C}_t$ matrices are not constant but time-varying and obtained from the linearization of a set of nonlinear functions ($\mathbf{f}_\Delta$ and $\mathbf{h}_\Delta$), the *Extended* version of the Kalman Filter was considered.

The EKF algorithm computes, for each discrete time instant t of integration ($t = 1, 2, \ldots$), a *prior* estimation of the unmeasurable states ($\mathbf{x}_t^-$) with Eq. (31), and corrects it with the bias between output's model predictions and real data (innovation, that enters the expression of the so-called Kalman gain $\mathbf{K}_t$), to postulate a *posterior* ($\mathbf{x}_t^+$) states' estimate, characterized by the $\mathbf{P}_t$ error covariance matrix of the estimate.

The filtering algorithm consists in a first *prediction* step (Eq.s (38) to (40)), and a consequent *correction* or *update* step (Eq.s (40) to (42)).

$$\hat{\mathbf{x}}_t^- = \mathbf{A}_{t-1} \hat{\mathbf{x}}_{t-1}^+ + \mathbf{B}_{t-1} \mathbf{u}_{t-1} \tag{38}$$

$$\mathbf{P}_t^- = \mathbf{A}_{t-1} \cdot \mathbf{P}_{t-1}^+ \cdot \mathbf{A}_{t-1}^T + \mathbf{Q} \tag{39}$$

$$\mathbf{K}_t = \mathbf{P}_t^- \cdot \mathbf{C}_t^T \cdot (\mathbf{C}_t \cdot \mathbf{P}_t^- \cdot \mathbf{C}_t^T + \mathbf{R})^{-1} \tag{40}$$

$$\mathbf{x}_t^+ = \mathbf{x}_t^- + \mathbf{K}_t \cdot (\tilde{\mathbf{y}}_t - \mathbf{C}_t \mathbf{x}_t^-) \tag{41}$$

$$\mathbf{P}_t^+ = (\mathbf{I} - \mathbf{K}_t \mathbf{C}_t) \cdot \mathbf{P}_t^- \tag{42}$$

The output values $\hat{\mathbf{y}}_t$ are computed evaluating the output-transformation function $\mathbf{h}_\Delta$ of Eq. (30) in $\mathbf{x}_t^+$ (and $\mathbf{u}_t$).

F. The selector-PI controller

The selector-PI scheme consists of equipping the q_M (expressed in L h^{-1}) PI controller with an override from the $x_{C,gb}/x_{M,gb}$ PI controller, to guarantee less inhibition-prone transients. The switch between the two PIs in the override structure is based on a hysteretic comparator that confronts the measured biogas ratio with a user-defined upper bound, and makes the output of the $x_{C,gb}/x_{M,gb}$ controller override that from the q_M one when the said bound is exceeded; the hysteresis serves to avoid unduly fast switching (see Figure S2).

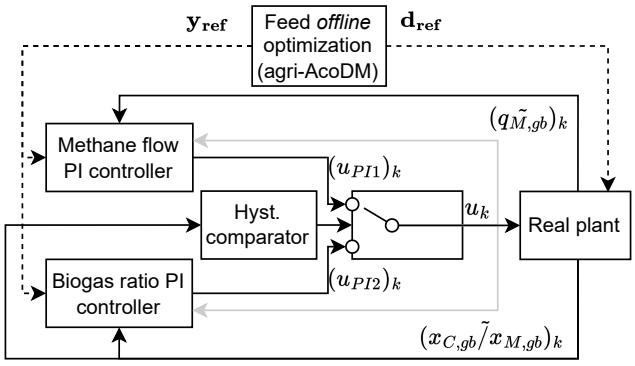

Fig. S2: Block diagram (contextualized to the case-study described in the main manuscript, Section 3.2) of the selector-PI control scheme used to control the 'Selector-PI' reactor. u_{PI1} and u_{PI2} are the control actions suggested by the methane flow (subscript 1) and biogas ratio (subscript 2) PIs respectively.

The control law of each PI is computed as detailed in Algorithm 1. In this framework, the *input* u corresponds to the control action generated by the active PI controller, while the Boolean variable TS is the output of the hysteretic comparator.

Input: k_P, T_I, T_c, u_{lb}, u_{ub}, u, y_{ref}, TS
Data: Integrator state $u_{I,0}$
for *each control step* k **do**
  $e \leftarrow y_{ref} - \tilde{y}$;
  $u_P \leftarrow k_P \cdot e$;
  if TS **then**
    $u_{PI} \leftarrow u_{TR}$;
  else
    $u_I \leftarrow u_{I,0} + \frac{k_P \cdot T_c}{T_I} \cdot e$;
    $u_{PI} \leftarrow u_P + u_I$;
  end
  $u_{PI} \leftarrow \max(u_{lb}, \min(u_{ub}, u_{PI}))$;
  $u_{I,0} \leftarrow u_{PI} - u_P$;
end

Algorithm 1: Discrete PI Controller with override and saturation.

Further details are reported in Carecci *et al.* [15]. The controller design parameters used in the experimental campaign subject of the main manuscript are reported in Table S9.

G. NMPC closed-loop

The NMPC control law is computed as the arg min of optimization problem defined by Eq.s (51)–(59) (*ancillary* problem). The *nominal* problem is instead described by Eq.s (43)–(50), where J is defined by Eq. (60).

$$\min_{\boldsymbol{\nu}\in\mathbb{V}} \quad J \tag{43}$$

$$\text{s.t.} \quad \dot{\mathbf{z}} = \mathbf{f}(\mathbf{z},\boldsymbol{\nu}), \quad \mathbf{z}\in\mathbb{Z}, \quad \boldsymbol{\nu}\in\mathbb{V} \tag{44}$$

$$\mathbf{y} = \mathbf{h}(\mathbf{z},\boldsymbol{\nu}) \tag{45}$$

$$\boldsymbol{\nu}_t = \boldsymbol{\nu}_{t_{0+H_c-1}}, \quad t\in[t_{0+H_c}, t_{0+H_p-1}] \tag{46}$$

$$\boldsymbol{\nu}_{\mathbf{lb}} \le \boldsymbol{\nu}_t \le \boldsymbol{\nu}_{\mathbf{ub}}, \quad t\in[t_0, t_{0+H_p-1}] \tag{47}$$

$$\Delta\boldsymbol{\nu}_{\mathbf{lb}} \le \Delta\boldsymbol{\nu}_t \le \Delta\boldsymbol{\nu}_{\mathbf{ub}}, \quad t\in[t_0, t_{0+H_c-2}] \tag{48}$$

$$\Delta\boldsymbol{\nu}\in\mathbb{DV} \tag{49}$$

$$\mathbf{z}_{\mathbf{lb}} \le \mathbf{z}_t \le \mathbf{z}_{\mathbf{ub}}, \quad t\in[t_0, t_{0+H_p-1}] \tag{50}$$

$$\min_{\mathbf{u}\in\mathbb{U},\ \mathbf{z}^*_{t_0}\in\mathbb{Z}} \quad \Big[w_{y_{Hp}}\Phi_{t_{0+Hp}} + \sum_{t=t_0}^{t_0+H_p-1} \left(w_x \left\|\mathbf{x}_t - \mathbf{z}^*_t\right\|_2 + w_u \left\|\mathbf{u}_t - \boldsymbol{\nu}^*_t\right\|_2\right)\Big] \tag{51}$$

$$\text{s.t.} \quad \dot{\mathbf{z}}^* = \mathbf{f}(\mathbf{z}^*,\boldsymbol{\nu}^*), \quad \mathbf{z}^*\in\mathbb{Z}, \quad \boldsymbol{\nu}^*\in\mathbb{V} \tag{52}$$

$$\dot{\mathbf{x}} = \mathbf{f}(\mathbf{x},\mathbf{u}), \quad \mathbf{x}\in\mathbb{X}, \quad \mathbf{u}\in\mathbb{U} \tag{53}$$

$$\mathbf{y} = \mathbf{h}(\mathbf{x},\mathbf{u}) \tag{54}$$

$$\mathbf{u}_t = \mathbf{u}_{t_{0+H_c-1}}, \quad t\in[t_{0+H_c}, t_{0+H_p-1}] \tag{55}$$

$$\mathbf{u}_{\mathbf{lb}} \le \mathbf{u}_t \le \mathbf{u}_{\mathbf{ub}}, \quad t\in[t_0, t_{0+H_p-1}] \tag{56}$$

$$\Delta\mathbf{u}_{\mathbf{lb}} \le \Delta\mathbf{u}_t \le \Delta\mathbf{u}_{\mathbf{ub}}, \quad t\in[t_0, t_{0+H_c-2}] \tag{57}$$

$$\Delta\mathbf{u}\in\mathbb{DU} \tag{58}$$

$$\mathbf{x}_{\mathbf{lb}} \le \mathbf{x}_t \le \mathbf{x}_{\mathbf{ub}}, \quad t\in[t_0, t_{0+H_p-1}] \tag{59}$$

$$J = \sum_{t=t_0}^{t_0+H_p-1} \Phi_t, \ \text{where } \Phi_t = \left\| \mathbf{y}_t - \mathbf{y}_{\mathbf{ref},t} \odot \frac{1}{\bar{\mathbf{y}}} \right\|_{2,\mathbf{W_y}} \tag{60}$$

Eq. (53) enforces the constraint of the model dynamics to start from the currently measured/estimated states of the real plant ($\tilde{\mathbf{x}}_t$ of Eq. (33) with $t = t_0$ of the optimization problem, i.e., the time index of the current k^{th} control step). The quantities introduced above are defined in the Glossary of the main manuscript. Further details can be found in Carecci *et al.* [16].

It should be noted that, from a theoretical standpoint (as originally described by Mayne *et al.* [49]), the bounded additive disturbances considered in the tube-based formulation—denoted as $\mathbf{w}$ in Carecci *et al.* [16]—do not correspond to the Gaussian process noise assumed in the EKF formulation (Eq. (33)). Rather, the tube-based NMPC framework requires disturbances to be bounded, i.e., $\mathbf{w}\in\mathbb{W}$, where $\mathbb{W}$ is a compact set containing the origin. In practice, parametric $\boldsymbol{\theta_{kin}}$ uncertainty was therefore interpreted as a bounded additive disturbance for control design, while Gaussian distributions were used to generate MC realizations for robustness assessment. The disturbance set $\mathbb{W}$ was selected to enclose high-probability realizations of the Gaussian uncertainty.

Note that, although the dimensionality of the EKF output vector is 3 (q_{TOT}, $x_{M,gb}$ and $x_{C,gb}$), the one of the output-related quantities present in the cost function of the NMPC optimization problem as defined in Carecci *et al.* [16] and $\mathbf{y_{ref}}$ is 2 ($q_{M,gb}$ and $x_{C,gb}/x_{M,gb}$). This apparent mismatch is intentional: in the EKF formulation, methane and carbon dioxide mole fractions were treated as separate outputs rather than as their ratio, in order to limit measurement-noise amplification. Indeed, the ratio of two noisy composition measurements exhibits a higher propagated uncertainty than the individual fractions, which are directly measured by the gas analyzer. The composition ratio was therefore computed only at the NMPC problem, where it enters the control objective. As a result, for $\mathbf{y_{ref}}$ (and, consistently, $\mathbf{W_y}$) it holds '(1)' index for $q_{M,gb,ref}$, the '(2)' for $(x_{C,gb}/x_{M,gb})_{ref}$.

Compared to the simulation studies previously conducted in Carecci *et al.* [16] and in Section 4.4 of the main manuscript, few settings of the real experiment during closed-loop operation differed and are recalled hereafter. First of all, the characterization of the feedstocks was updated coherently with the new measurements available, and, most importantly, the feeding frequency of $\mathbf{d_{ref}}$ was daily instead of 3 times per week; Moreover, in light of the transient inhibition observed

before closed-loop operation (15-27/04/2025), occurring shortly after the full initial load was reached (7/04/2025, following inoculum adaptation), the controller was re-tuned in a slightly more conservative, robustness-oriented manner prior to the experimental campaign, with:

- a slightly tighter upper-bound for the TVFA in the *nominal* problem ($S_{2,ub}$ = 15 instead of 20 mmol L^{-1});
- a slightly lower weight on the $(x_{C,gb}/x_{M,gb})_{ref}$ tracking in the cost functions (tuning hyper-parameter $W_y^{(2)}$ = 0.8 instead of 1);
- a slightly lower weight to the tracking of the states' trajectories ($\mathbf{z}^*$) computed by the *nominal* problem into the cost function of the *ancillary* one (tuning hyper-parameter w_x = 0.8 instead of 1).

Finally, since during the initial equilibrium period the average $x_{C,gb}/\tilde{x}_{M,gb}$ was slightly lower than the reference value suggested by the *offline* optimization, the time-varying $(x_{C,gb}/x_{M,gb})_{ref}$ was converted into a constant value (0.85), instead of a trajectory starting in 0.88, peaking at 0.92 on the *transient* period and terminating at 0.90 during the final equilibrium. This choice was meant to limit any NMPC action potentially resulting in higher $x_{C,gb}/x_{M,gb}$ values. The final controller design parameters used in the experimental campaign are reported in Table S9.

TABLE S9: Controllers' design parameters values (hyper-parameters). $d\mathrm{u}_{lb}$ and $d\mathrm{u}_{ub}$ are named like that since the PI controllers actually compute the u deviation/correction with respect to the linearization point, i.e. the initial equilibrium (in practice, the feedforward u_0 is added to the output of the PI controller blocks to compute the actual control action).

***Online* tube-based NMPC**	
T_c (h)	$\min(\Delta T, 6)$
Δu_{lb} (g_{FM} d^{-1})	-50
Δu_{ub} (g_{FM} d^{-1})	50
u_{lb} (g_{FM} d^{-1})	0
u_{ub} (g_{FM} d^{-1})	250
H_p (*control steps*)	10
H_c (*control steps*)	2
w_x (-)	0.8
w_u (-)	0.1
$w_{y_{H_p}}$ (-)	1
$W_y^{(1)}$ (-)	1
$W_y^{(2)}$ (-)	0.8
$w_{\boldsymbol{\varepsilon}_{lb}}$ (-)	1'000
$w_{\boldsymbol{\varepsilon}_{ub}}$ (-)	1'000
Selector-PI	
T_c (h)	3
$d\mathrm{u}_{lb}$ (g_{FM} d^{-1})	-99.00
$d\mathrm{u}_{ub}$ (g_{FM} d^{-1})	150.00
$k_{P,1}$ (-)	$6.80e^{-4}$
$k_{P,2}$ (-)	$4.57e^{-3}$
$T_{I,1}$ (-)	$1.45e^{5}$
$T_{I,2}$ (-)	$9.23e^{4}$
$(x_{C,gb}/x_{M,gb})_{ub,low}$ (-)	$(x_{C,gb}/x_{M,gb})_{ref}$ + 0.05
$(x_{C,gb}/x_{M,gb})_{ub,high}$ (-)	$(x_{C,gb}/x_{M,gb})_{ref}$ + 0.1

H. Practical control implementation

The agri-AcoDM was developed in OpenModelica using the Modelica language, i.e. an open-source, high-level, declarative and object-oriented modeling language [51]. The resulting library can be download from this GitHub repository. The *offline* optimization problem was solved using the Differential Evolution (DE) algorithm embedded in the SciPy Python library, with the agri-AcoDM integrator executed through the OpenModelica Compiler (OMC) invoked as a Python *subprocess*. The $\mathrm{AM2HN}_{obs}$ model and the related EKF and NMPC modules were implemented using both the SciPy and CasADi libraries. The *online* optimization problems, formalized with the multiple-shooting approach, were solved with the Interior Point OPTimizer (IPOPT) solver (average computation time of 1-2 min).

The closed-loop architecture was set up around the above-mentioned reactors and sensors with the aid of (i) a local network (router), (ii) an RJ45 cable connecting the AwiLAB hardware to a Raspberry Pi 4B to allow for the serial communication of the *online* data via Modbus protocol, (iv) a GPIO-relay board able to withstand high voltage/high loads, and (v) peristaltic pumps (Seko S.p.A., Rieti, Italy) as actuators (see Figure 4 in the main manuscript text). It is important to stress that the full-scale applicability of the proposed methods is embedded in the $\mathrm{AM2HN}_{obs}$ model by the fact that no other *online* measurement is considered except for biogas flow rate and composition. Indeed, the other quantities monitored *offline* were not measured with enough frequency to be consistent with the control intervals (T_c = 6 and 3 h for the NMPC and selector-PI controller respectively) and the open-loop model/EKF integration step (Δt = 5 min).

The biogas flow rate data were preprocessed by removing outliers (6σ-rule) and applying a moving average over 12 data points (corresponding to a 1 h window). Since biogas composition analysis could be performed only after the accumulation of 4.5 L, a new measurement became available approximately every 6 h, which was sufficient to treat $x_{C,gb}/x_{M,gb}$ as an *online* information. Between successive analyses, a sample-and-hold assumption was adopted to maintain consistency with Δt. However, since infra-daily biogas production was not constant, these analyses were not synchronized with the control steps: to address this, a 1-hour frequent *cronjob* (i.e. an automatically scheduled system task executed at predefined time intervals) was executed to check for newly available biogas composition data and, if detected, immediately trigger a new NMPC execution. This, in practice, resulted in an asynchronous NMPC with time-varying control interval given by $T_c = \min(\Delta T; 6)$, where ΔT denotes the elapsed time since the last biogas composition measurement. Consistently, the multi-step ahead predictions addressed in this work had $multi = T_c/\Delta t, \in [12, 72]$, i.e. 1–6 h, depending on T_c and ΔT.

The manual feeding of $\mathbf{d_{ref}}$ was approximated as 5-minute pulse inputs, matching the integration time step (the pulse magnitude was determined by multiplying the daily load by 86'400/300 seconds). During real-time operations, the $\mathbf{d_{ref}}$ schedule was updated daily with the actual mass fed. Feeding times were provided via a CSV file (with a $\pm$ 10 minutes accuracy) and processed by the Python control routines. Given that the above-mentioned cronjob was executed hourly at the beginning of each hour, feeding events were intentionally scheduled sufficiently far from the hour mark to avoid timing conflicts with updated code execution. A similar approach was considered for feedstocks' characterization updates (TS and VS only, as described in Section II-C).

The major hyper-parameters values of both controllers are reported in Table S9. Considering the relevant modeling uncertainty and disturbances given by the impulse manual feeding, slack variables ($\boldsymbol{\varepsilon_{lb}}, \boldsymbol{\varepsilon_{ub}}$) were added to the *nominal* NMPC problem (weighted by $w_{\boldsymbol{\varepsilon}_{lb}}$ and $w_{\boldsymbol{\varepsilon}_{ub}}$ in the cost function) re-formulating (softening) the state bound constraints as for Eq. (61).

$$\mathbf{z_{lb}} - \boldsymbol{\varepsilon_{lb}} \leq \mathbf{z}_t \leq \mathbf{z_{ub}} + \boldsymbol{\varepsilon_{ub}}, \quad t \in [t_0, t_{0+H_p-1}] \tag{61}$$

To guarantee the desired degree of safety, the main tightening of the states' feasible sets in the *nominal* problem of the NMPC was enforced on the upper bound of TVFA (15 mmol L^{-1}) and the lower bounds of the methanogens' concentration (1 g L^{-1}) and the biogas' methane content (0.5). All states' bounds ($\mathbb{X}$ and $\mathbb{Z}$) are reported in Table S5. The input feasible sets $\mathbb{U}$ (and $\mathbb{DU}$) were set from the actual peristaltic pump saturation (values reported in Table S9). No tightening for the sets of the *nominal* NMPC problem ($\mathbb{V}$ and $\mathbb{DV}$) was applied. At each control step, the scalar control action u was mapped to a pulse-width modulated (PWM) signal, where the duty cycle determined the ON/OFF switching times of the relay.

In the real closed-loop, the overall execution time required to run the tube-based NMPC Python file (data preprocessing, EKF, IPOPT optimizations of the *nominal* and *ancillary* NMPC problems, plotting) at each control step was $\approx$ 10 minutes (6-36 times lower than T_c, depending on ΔT). The number of iterations required by the IPOPT solver was normally between 10 and 20.

III. Results

A. Models' performances

The practical identifiability analysis of the AM2HN$_{obs}$ $\boldsymbol{\theta_P}$, conducted on data collected during the first weeks of the experiment (i.e., prior to closed-loop operation), indicated that only the parameters k_5 and k_6 could be reliably updated, whereas $\mu_{max,2}$ and $K_{S,2}$ would be associated with high uncertainty. Since the open-loop model performance over the same period was deemed satisfactory, no parameter re-estimation was performed. This choice allowed the entire dataset from the current experiment to be preserved for model validation purposes.

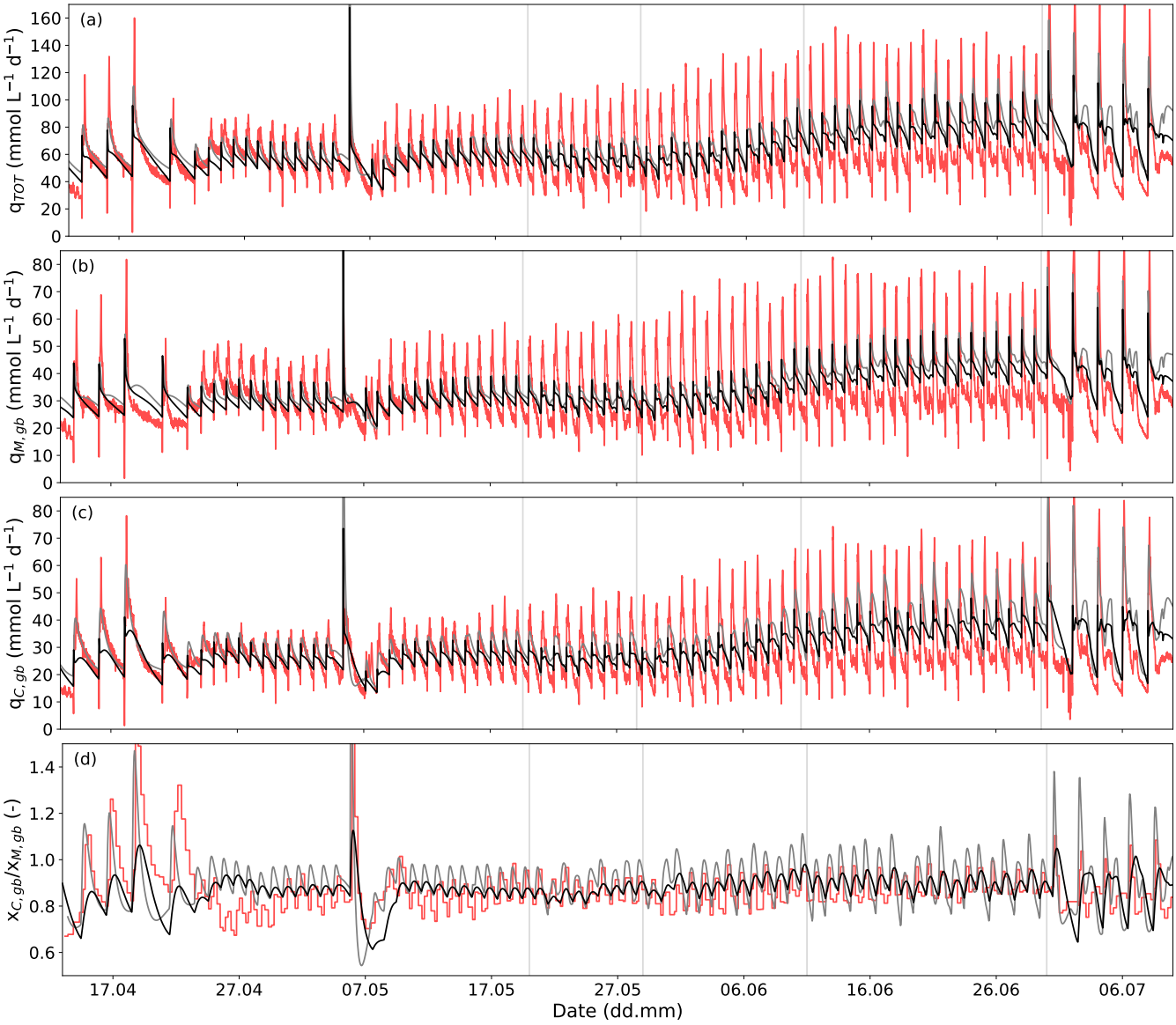

Fig. S3: The models' performances over the real *online* data: agri-AcoDM (black) against AM2HN$_{obs}$ (grey). Vertical dashed gray lines report the start of the closed-loop, start-end of the ramping period, and the start of the final period with $\mathbf{d_{ref}}$ feeding every 2 days. An acetate pulse was applied on 05/05/2025 to validate the estimated Haldane parameters and increase data informativeness for potential re-estimation (not performed).

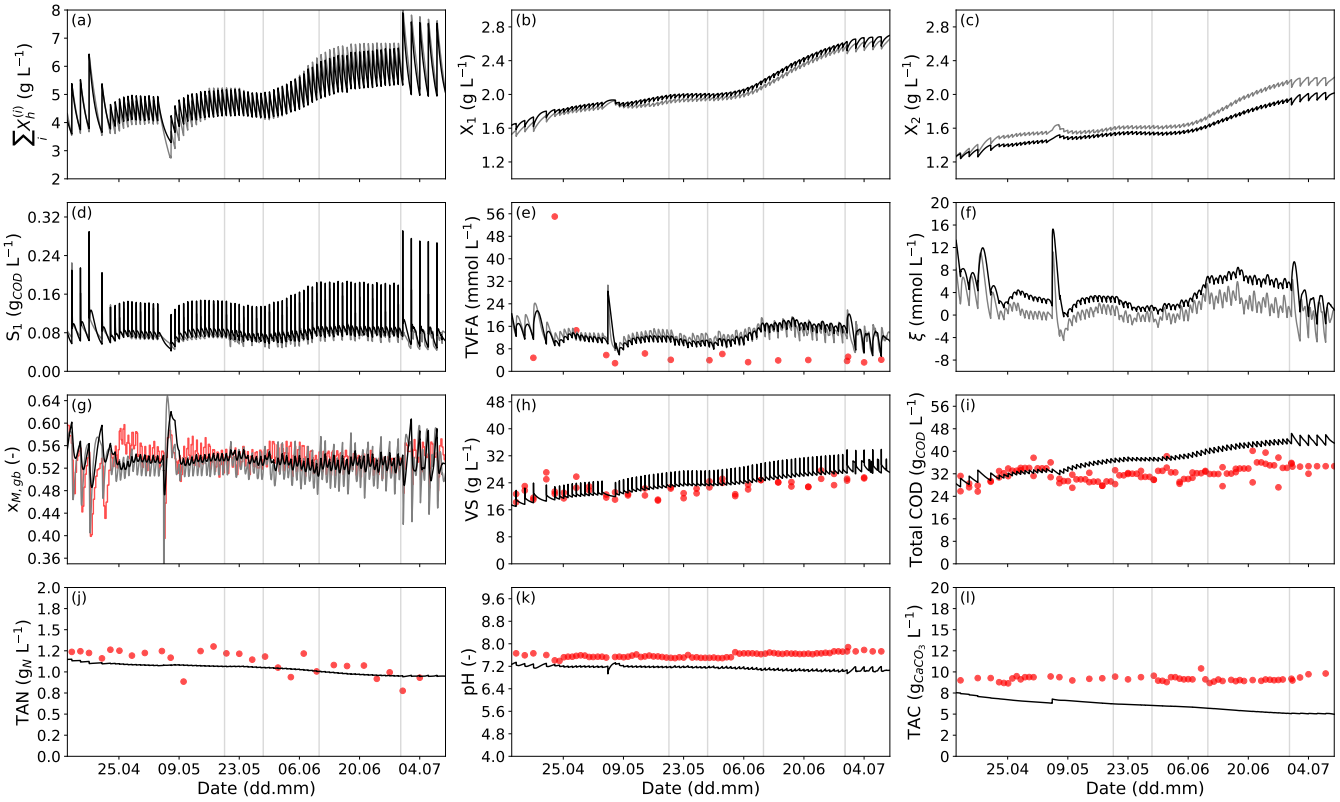

Fig. S4: From (a) to (g): open-loop AM2HN$_{obs}$ (grey) and agri-AcoDM (black) predictions' matching over the simulation of the real experiment (where present, real data are shown in red). From (h) to (l): open-loop agri-AcoDM model (black) performances over the *offline* data of the real experiment (red).

B. EKF tuning

TABLE S10: Averages and standard deviations over the 400 MC runs of the EKF estimation's MARE$_{\%}$, r^2 and MAE, with respect to the true state, for all states (robustness analysis of the EKF design to $\hat{\mathbf{x}}_0$ and $\boldsymbol{\theta}_{kin}$ uncertainties; step response (Figure 5 in the main manuscript)).

	$\bar{\text{MARE}}_{\%}$	$\bar{r^2}$	$\bar{\text{MAE}}$
$X_h^{(1)}$ (g_{VS} L^{-1})	3.58 ± 2.91	0.71 ± 0.29	0.07 ± 0.06
$X_h^{(2)}$ (g_{VS} L^{-1})	6.45 ± 5.27	0.81 ± 0.27	0.10 ± 0.08
$X_h^{(3)}$ (g_{VS} L^{-1})	3.28 ± 2.18	0.87 ± 0.19	0.01 ± 0.01
X_1 (g_{VS} L^{-1})	10.15 ± 8.30	0.81 ± 0.27	0.16 ± 0.13
X_2 (g_{VS} L^{-1})	9.22 ± 6.29	0.78 ± 0.22	0.12 ± 0.08
S_1 (g_{COD} L^{-1})	14.52 ± 10.97	0.19 ± 0.20	0.01 ± 0.01
S_2 (mmol L^{-1})	5.57 ± 4.28	0.70 ± 0.24	0.77 ± 0.59
ξ (mmol L^{-1})	78.01* ± 62.05	0.76 ± 0.24	0.75 ± 0.59
$x_{M,gb}$ (-)	0.77 ± 0.01	-	0.00 ± 0.00

**very high because the true state values are near 0.*

C. Comparison between the two controllers: 'NMPC' vs 'Selector-PI'

The comparison between the two controllers' control actions and tracking is shown in Figure S5 and Figure S6 respectively, and quantified in Table S11. In this respect, given the intrinsic complexity of the bioprocess and the practical challenges of bench-scale experimentation (e.g., manual feeding of TS-rich co-feedstocks, measurement noise, and non-ideal actuation), drawing high-confidence conclusions is nontrivial, especially considering the relatively small differences observed between the outputs of the two reactors. Qualitatively, it can be stated that the NMPC managed to reproduce almost the same biomethane flow rate tracking of the selector-PI, with smoother control actions and while maintaining slightly more stable/safer system's responses, especially in terms of both lower $x_{C,gb}/\tilde{x}_{M,gb}$ and TVFA oscillations, maximum values and frequency of occurrence of higher values [16], as can be deduced from Figure S7.

TABLE S11: Quantification/metrics of the controllers' performances in closed-loop operation.

	Time window*	**Biomethane flow rate**		**Biogas composition ratio**		**Control action****
	(dd/mm - dd/mm)	$\mathbf{q}_{\mathbf{M,gb}}$ (mmol d^{-1} L^{-1})	**MARE**$_{\%}$	$\mathbf{x}_{\mathbf{C,gb}}/\bar{\bar{\mathbf{x}}}_{\mathbf{M,gb}}$ (-)	**MARE**$_{\%}$	$\bar{\mathbf{u}}$ (g$_{FM}$ L^{-1})
'NMPC'	20/05 - 29/05	31.10	28.55	0.866	5.12	86.13 (92.15)
	21/06 - 30/06	36.25	26.78	0.889	5.45	138.0 (113.8)
	20/05 - 30/06	34.38	29.84	0.869	5.47	104.8 (96.92)
'Selector-PI'	20/05 - 29/05	30.50	20.75	0.863	6.03	82.34 (90.26)
	21/06 - 30/06	37.28	25.16	0.882	6.99	92.93 (96.18)
	20/05 - 30/06	34.62	24.33	0.874	7.11	87.25 (89.56)

**20/05–29/05: initial equilibrium; 21/06–30/06: final equilibrium; 20/05–30/06: overall closed-loop period with daily feeding.*

***the $\bar{u}$ value within brackets is the amount actually fed by the peristaltic pumps (net of actuation's imperfections).*

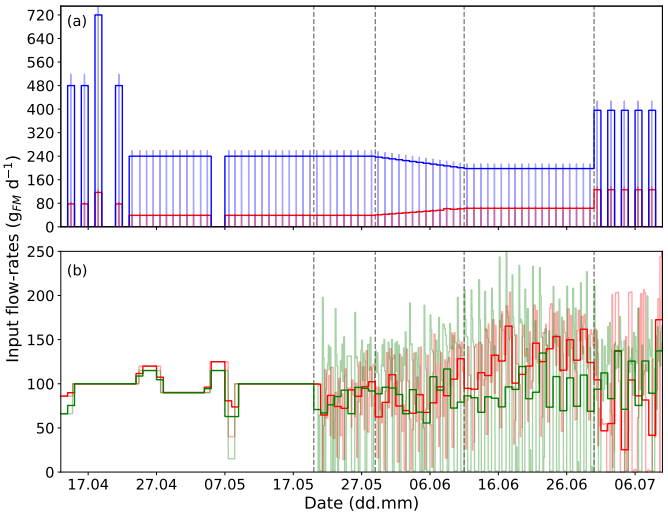

Fig. S5: Daily loads of the real experiment. In (a): $\mathbf{d_{ref}}$ loads of maize silage (red) and cow slurry (blue). Feeding instants are also shown with clearer lines. In (b): tomato sauce dosages requested to the pumps of the 'NMPC' (red) and 'Selector-PI' (green) reactors (closed-loop control actions from 20/05/2025). Vertical dashed gray lines report the start of the closed-loop, start-end of the ramping period, and the start of the final period with $\mathbf{d_{ref}}$ feeding every 2 days.

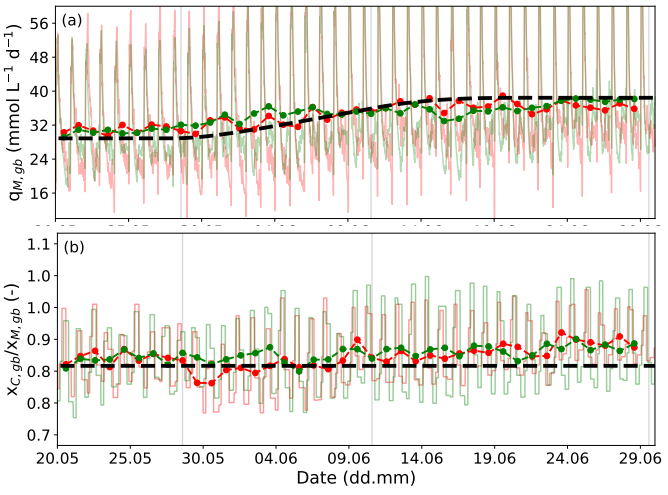

Fig. S6: Tracking of $\mathbf{y_{ref}}$ (black dashed lines) by the 'NMPC' (red) and 'Selector-PI' (green) reactors over closed-loop operations. Real data are shown as clearer lines, whereas the daily averages are shown as dashed thicker lines with markers.

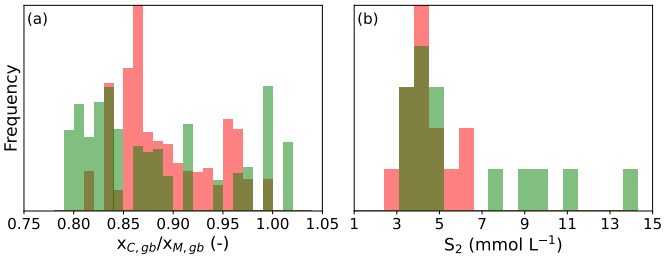

Fig. S7: Histogram to compare the distributions of: (a) the $x_{C,gb}/\tilde{x}_{M,gb}$ and (b) the $\tilde{S}_2$ data of the 'NMPC' (red) and 'Selector-PI' (green) reactors, measured over the closed-loop operations.

To support this assertion, Figure S8 zooms in Figure S6 to show the different strategies of the two controllers in dealing with the $\mathbf{d}_{\mathbf{ref}}$ impulse feeding (infra-day behaviors): as the latter is unknown to the selector-PI, as soon as the $x_{C,gb}/\tilde{x}_{M,gb}$ stability proxy decreases below the threshold, tomato sauce is heavily dosed to "cover" the missing $q_{\tilde{M},gb}$ with respect to $q_{M,gb,ref}$ (during the discharge phase of the $\mathbf{d}_{\mathbf{ref}}$ response), until the next feeding pulse leads $q_{\tilde{M},gb}$ and $x_{C,gb}/\tilde{x}_{M,gb}$ to peak again. During these peaks, contrary to the capability of the NMPC to predict in the near future, the selector-PI saturated to null loads, as its only and best way to reject the $\mathbf{d}_{\mathbf{ref}}$ effects. As a result, the selector-PI had a much stronger *bang-bang* behavior with respect to the tube-based NMPC that, inversely, tended to reduce the control action just before the known next pulse of $\mathbf{d}_{\mathbf{ref}}$ to reduce the distance of the impulse response's peak to $\mathbf{y}_{\mathbf{ref}}$.

However, apparently, the selector-PI presented a slightly better $q_{\tilde{M},gb}$ tracking and specific biomethane production at the optimized final equilibrium (292.0 and 272.7 NmL_{CH_4}/g_{VS} for 'Selector-PI' and 'NMPC' respectively). Considering the higher dynamism of the selector-PI u trajectory, this result may be justified by the presence of non-trivial microbial responses: in some works, less frequent feeding or pulse feeding is stated to create temporal niches (e.g. variable acetate/TVFA concentrations) that may allow competing microbial species to coexist, thus increasing biodiversity, redundancy and the functional resilience of the microbial community, sometimes giving higher biomethane yields and tolerance to perturbations (shock load, inhibitors) [13]. However, such consideration may hold true only if the system has sufficient buffering capacity, and it is operated far from potential crashing conditions (such as inhibition or microbial biomass wash out).

As a consequence of the robustness-oriented tuning of the *online* tube-based NMPC, and given that no inhibition occurred during the diet transient, the present experiment suggests that the selector-PI operated under less restrictive conditions (less safe operations in terms of TVFA and CO_2/CH_4 stability proxies), achieved slightly better biomethane flow rate tracking and feedstock utilization. However, since the NMPC explicitly enforced a TVFA upper bound, thereby incorporating stronger stability guarantees, the comparison between the two biomethane production trackings is inherently asymmetric. The resulting conclusions should therefore be interpreted as qualitative rather than definitive.

Independently of the comparison between the two controllers—which was a secondary objective of the present study—the developed model-based predictive framework offers clear advantages for process monitoring (when coupled with the estimation of unmeasurable states) and subsequent scenario analysis. From a full-scale application perspective, the controller would not be required to handle such large and discrete $\mathbf{d}$ feeding events. Industrial facilities are typically equipped with screw-press or dosing systems that substantially increase the feeding frequency of TS-rich substrates and allow automated operation, thereby approximating quasi-continuous feeding conditions. Indeed, an additional advantage of the NMPC lies in its straightforward extension to a MIMO configuration, in contrast to the selector-PI strategy, whose scalability is inherently limited.

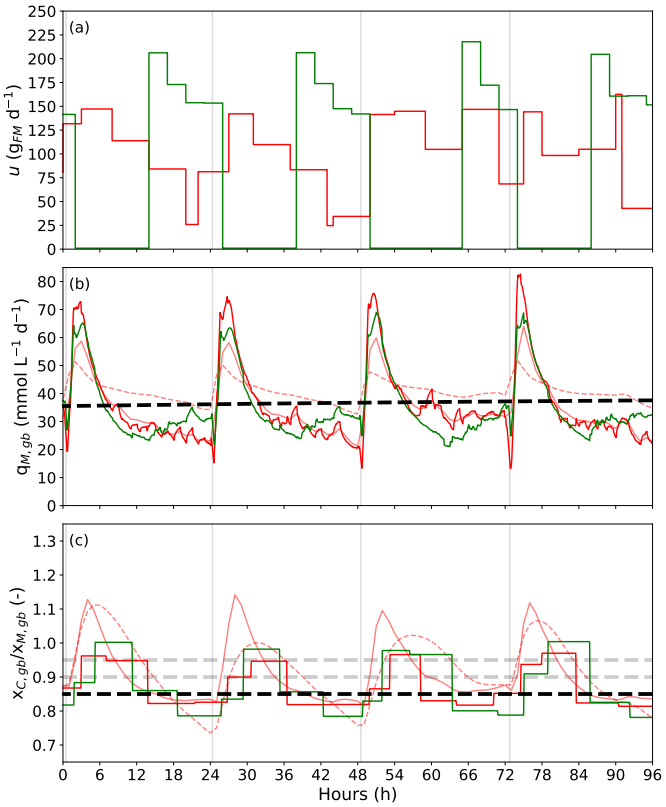

Fig. S8: Zoom (4 days from 10/06/2025 10AM) of the closed-loop behaviors of the 'NMPC' (red) and 'Selector-PI' (green) reactors. $\mathbf{y_{ref}}$ as black dashed lines; selector-PI hysteresis region for the $x_{C,gb}/x_{M,gb}$'s upper bound is delimited by gray dashed lines. For 'NMPC' (red-like shades), the EKF corrections (continuous lines) and open-loop AM2HN$_{obs}$ model's predictions (dashed lines) are also shown.

D. Practical observability analysis

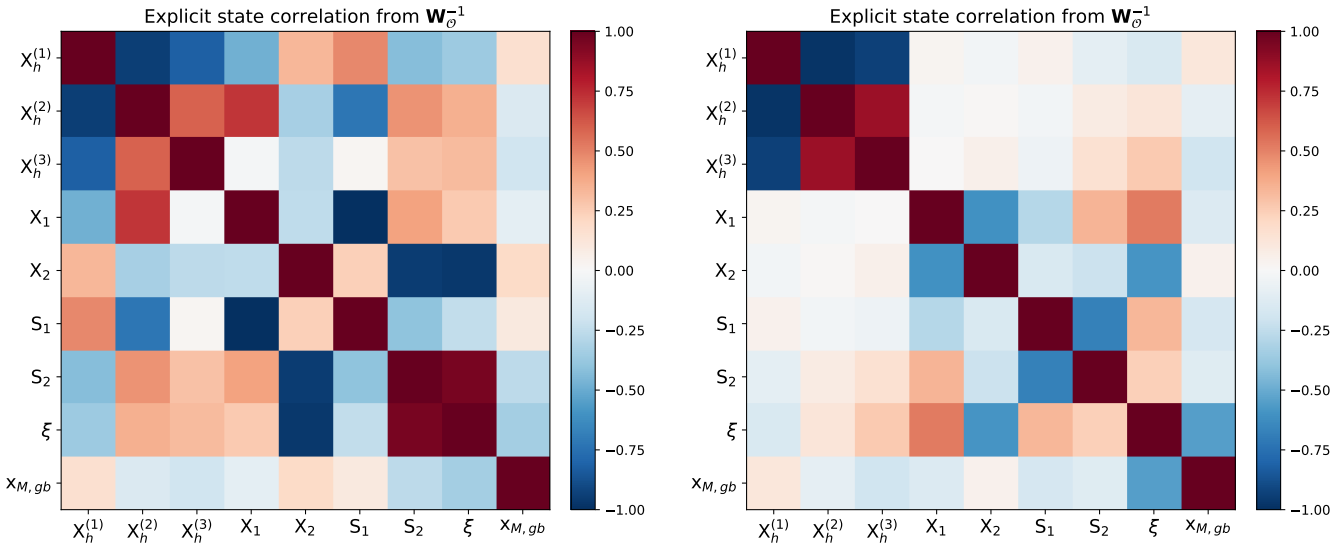

Fig. S9: Correlation matrix from the $\mathbf{W}_{\mathcal{O}}$ inverse: (left) simple step response, (right) input profile of the experiment described in Carecci *et al.* [15] (results reported in Carecci *et al.* [17]).

REFERENCES

[1] Cesar-Arturo Aceves-Lara, Eric Latrille, and Jean-Philippe Steyer. Optimal control of hydrogen production in a continuous anaerobic fermentation bioreactor. *International Journal of Hydrogen Energy*, 35(19):10710–10718, 2010. Indo-French Workshop on Biohydrogen: from Basic Concepts to Technology.

[2] Wasim Ahmed and Jorge Rodríguez. A model predictive optimal control system for the practical automatic start-up of anaerobic digesters. *Water Research*, 174:115599, 2020.

[3] V. Alcaraz-Gonzalez, E.A. Jauregui-Medina, J.Ph. Steyer, J.P. García-Sandoval, H.O. Méndez-Acosta, and V. Gonzalez-Alvarez. Simultaneous cod and vfa unmeasured process inputs estimation in actual anaerobic wastewater treatment processes. *Control Engineering Practice*, 60:118–123, 2017.

[4] V. Alcaraz-González, J. Harmand, A. Rapaport, J.P. Steyer, V. González-Álvarez, and C. Pelayo-Ortiz. Robust interval-based regulation for anaerobic digestion processes. *Water Science and Technology*, 52(1-2):449–456, 07 2005.

[5] Víctor Alcaraz-González, Rubén Horacio López-Bañuelos, Jean-Philippe Steyer, Hugo Oscar Méndez-Acosta, Víctor González-Álvarez, and Carlos Pelayo-Ortiz. Interval-based diagnosis of biological systems – a powerful tool for highly uncertain anaerobic digestion processes. *CLEAN – Soil, Air, Water*, 40(9):941–949, 2012.

[6] Stéphanie Aparicio, Josué González-Camejo, Aurora Seco, Luis Borrás, Ángel Robles, and José Ferrer. Integrated microalgae-bacteria modelling: application to an outdoor membrane photobioreactor (mpbr). *Science of The Total Environment*, 884:163669, 2023.

[7] APHA, AWWA, and WEF. *Standard Methods for the Examination of Water and Wastewater*. American Public Health Association, Washington, DC, 22 edition, 2012.

[8] Shadi Attar and Finn Haugen. Comparison of different state estimator algorithms applied to a simulated anaerobic digestion reactor. In *Proceedings of The 59th Conference on Simulation and Modelling (SIMS 59)*, pages 118–125, 11 2018.

[9] Michel Azúa-Poblete, Angel L. Cedeño, Juan C. Agüero, Lino O. Santos, Laurent Dewasme, Alain Vande Wouwer, and Santiago García-Gen. Enhancing anaerobic digestion performance with offset-free model predictive control. *Journal of Water Process Engineering*, 78:108785, 2025.

[10] Ruijie Bai, Xiaojue Li, and Naoto Shimizu. Development of a fed-batch-scale anaerobic co-digestion control system based on multivariable output error state space and model predictive control. *Results in Engineering*, 22:102284, 2024.

[11] Damien Batstone and Xavier Flores-Alsina. *Generalised Physicochemical Model (PCM) for Wastewater Processes*. IWA Publishing, 11 2022.

[12] {Damien J.} Batstone, Daniel Puyol, Xavier {Flores Alsina}, and Jorge Rodríguez. Mathematical modelling of anaerobic digestion processes: applications and future needs. *Reviews in Environmental Science and Biotechnology*, 14:595–613, 2015.

[13] Fabian Bonk, Denny Popp, Sören Weinrich, Heike Sträuber, Sabine Kleinsteuber, Hauke Harms, and Florian Centler. Intermittent fasting for microbes: how discontinuous feeding increases functional stability in anaerobic digestion. *Biotechnology for Biofuels*, 11, 10 2018.

[14] D. Carecci, A. Catenacci, S. Rossi, F. Casagli, G. Ferretti, A. Leva, and E. Ficara. A plant-wide modelling framework to describe microalgae growth on liquid digestate in agro-zootechnical biomethane plants. *Chemical Engineering Journal*, 485:149981, 2024.

[15] Davide Carecci, Arianna Catenacci, Elena Ficara, Gianni Ferretti, and Alberto Leva. Modelling, optimisation and control of full-scale co-digestion biomethane plants. In *2024 IEEE 63rd Conference on Decision and Control (CDC)*, pages 106–112, 2024.

[16] Davide Carecci, Laurent Dewasme, Alessio La Bella, Gianni Ferretti, and Alain Vande Wouwer. Tube-based robust nonlinear model predictive control of anaerobic co-digestion. In *2025 IEEE 64th Conference on Decision and Control (CDC)*, pages 6466–6473, 2025.

[17] Davide Carecci, Giulia Quarta, Arianna Catenacci, Gianni Ferretti, and Elena Ficara. Modelling of agro-zootechnical anaerobic co-digestion for full-scale applications. In *Systems and Control Transactions*, volume 4, pages 2310–2315. PSE Press, 07 2025.

[18] K. Chaib Draa, A. Zemouche, M. Alma, H. Voos, and M. Darouach. A discrete-time nonlinear state observer for the anaerobic digestion process. *International Journal of Robust and Nonlinear Control*, 29(5):1279–1301, 2019.

[19] Luis G. Cortés, J. Barbancho, D. F. Larios, J. D. Marin-Batista, A. F. Mohedano, C. Portilla, and M. A. de la Rubia. Full-scale digesters: Model predictive control with online kinetic parameter identification strategy. *Energies*, 15(22), 2022.

[20] L. Dewasme, M. Sbarciog, E. Rocha-Cózatl, F. Haugen, and A. Vande Wouwer. State and unknown input estimation of an anaerobic digestion reactor with experimental validation. *Control Engineering Practice*, 85:280–289, 2019.

[21] Xavier Flores-Alsina, Kimberly Solon, Christian Kazadi Mbamba, Stephan Tait, Krist V. Gernaey, Ulf Jeppsson, and Damien J. Batstone. Modelling phosphorus (p), sulfur (s) and iron (fe) interactions for dynamic simulations of anaerobic digestion processes. *Water Research*, 95:370–382, 2016.

[22] Hilario Flores-Mejia, Antonio Lara-Musule, Eliseo Hernández-Martínez, Ricardo Aguilar-López, and Hector Puebla. Indirect monitoring of anaerobic digestion for cheese whey treatment. *Processes*, 9(3), 2021.

[23] D. Gaida, C. Wolf, C Meyer, A. Stuhlsatz, J Lippel, T. Bäck, M. Bongards, and S. McLoone. State estimation for anaerobic digesters using the adm1. *Water Science and Technology*, 66(5):1088–1095, 2012.

[24] Daniel Gaida, Christian Wolf, Thomas Bäck, and Michael Bongards. Nonlinear model predictive substrate feed control of biogas plants. In *2012 20th Mediterranean Conference on Control & Automation (MED)*, pages 652–657. IEEE, 2012.

[25] Santiago García-Gen, Lino O Santos, and Alain Vande Wouwer. Application of a nonlinear model predictive controller to the anaerobic digestion of readily biodegradable wastes. *IFAC-PapersOnLine*, 55(7):909–914, 2022.

[26] Santiago García-Gen, Jorge R., and Juan Lema. Control strategy for maximum anaerobic co-digestion performance. *Water Research*, 80:209–216, 09 2015.

[27] Santiago García-Gen and Alain Vande Wouwer. A model-based optimisation strategy for the start-up of anaerobic co-digestion processes. *Renewable Energy*, 170:693–702, 2021.

[28] Mohammad Amin Ghanavati, Ehsan Vafa, and Mohammad Shahrokhi. Control of an anaerobic bioreactor using a fuzzy supervisory controller. *Journal of Process Control*, 103:87–99, 2021.

[29] C.P. Guillén-Flores, B. Castillo-Toledo, J.P. García-Sandoval, S. Di Gennaro, and V. González Álvarez. A reset observer with discrete/continuous measurements for a class of fuzzy nonlinear systems. *Journal of the Franklin Institute*, 350(8):1974–1991, 2013.

[30] Yang Haifeng, Deng Rui, Jin Junwei, Wu Yuling, Jiang Xin, and Shi Jinhua. Hydrolytic performances of different organic compounds in different lignocellulosic biomass during anaerobic digestion. *Environmental Engineering Research*, 27(4):210013–0, 2022.

[31] HANNA Instruments. Ammonia nitrogen (nessler) method. Technical method description, 2020. Adapted from ASTM D1426 and *Standard Methods for the Examination of Water and Wastewater*, Method 4500-NH_3.

[32] S. Hassam, E. Ficara, A. Leva, and J. Harmand. A generic and systematic procedure to derive a simplified model from the anaerobic digestion model No. 1 (ADM1). *Biochemical Engineering Journal*, 99:193–203, 2015.

[33] Finn Haugen, Rune Bakke, and Bernt Lie. State estimation and model-based control of a pilot anaerobic digestion reactor. *Journal of Control Science and Engineering*, 2014(1):572621, 2014.

[34] Dingxin He, Haoping Wang, Yang Tian, Nicolai Christov, and Ivan Simeonov. Trajectory tracking of two-stage anaerobic digestion process: A predictive control with guaranteed performance and saturated input, based on ultra-local model. *Journal of Process Control*, 129:103039, 2023.

[35] Simon Hellmann, Julius Frontzek, David M. Zarate, Terrance Wilms, Konrad Koch, Steffi Knorn, Stefan Streif, and Sören Weinrich. Multi-stage model predictive control of agricultural anaerobic digestion plant with uncertain substrate characterization. *Bioresource Technology*, 441:133568, 2026.

[36] Simon Hellmann, Arne-Jens Hempel, Stefan Streif, and Sören Weinrich. Observability and identifiability analyses of process models for agricultural anaerobic digestion plants. In *2023 24th International Conference on Process Control (PC)*, pages 84–89, 2023.

[37] E. A. Jáuregui-Medina, V. Alcaraz-González, H. O. Méndez-Acosta, and V. González-Álvarez. Observer-based input estimation in continuous anaerobic wastewater treatment processes. *Water Science and Technology*, 60(3):805–812, 07 2009.

[38] Hoil Kil, Dewei Li, Yugeng Xi, and Jiwei Li. Model predictive control with on-line model identification for anaerobic digestion processes. *Biochemical Engineering Journal*, 128:63–75, 2017.

[39] Wolf Klöckner, Riad Gacem, Tibor Anderlei, Nicole Raven, Stefan Schillberg, Clemens Lattermann, and Jochen Büchs. Correlation between mass transfer coefficient kla and relevant operating parameters in cylindrical disposable shaken bioreactors on a bench-to-pilot scale. *Journal of biological engineering*, 7:28, 12 2013.

[40] Konrad Koch, Manfred Lübken, Tito Gehring, Marc Wichern, and Harald Horn. Biogas from grass silage – measurements and modeling with adm1. *Bioresource Technology*, 101(21):8158–8165, 2010.

[41] Matthias Körber, Sören Weinrich, Roland Span, and Mandy Gerber. Demand-oriented biogas production to cover residual load of an electricity self-sufficient community using a simple kinetic model. *Bioresource Technology*, 361:127664, 2022.

[42] Gerardo Lara-Cisneros, Ricardo Aguilar-López, Denis Dochain, and Ricardo Femat. On-line estimation of vfa concentration in anaerobic digestion via methane outflow rate measurements. *Computers & Chemical Engineering*, 94:250–256, 2016.

[43] Gerardo Lara-Cisneros and Denis Dochain. Software sensor for online estimation of the vfa's concentration in anaerobic digestion processes via a high-order sliding mode observer. *Industrial & Engineering Chemistry Research*, 57(42):14173–14181, 2018.

[44] Dan Li, Ingyu Lee, and Hyunook Kim. Application of the linearized adm1 (ladm) to lab-scale anaerobic digestion system. *Journal of Environmental Chemical Engineering*, 9(3):105193, 2021.

[45] Hongxuan Li, Yang Tian, Haoping Wang, Ivan Simeonov, and Nicolai Christov. A volatile fatty acids adaptive observer-based hierarchical optimal controller design to maximum gas production of two-stage anaerobic digestion process. *Computers & Chemical Engineering*, 181:108524, 2024.

[46] I. López and L. Borzacconi. Modelling a full scale uasb reactor using a cod global balance approach and state observers. *Chemical Engineering Journal*, 146(1):1–5, 2009.

[47] Manfred Lübken, Marc Wichern, Markus Schlattmann, Andreas Gronauer, and Harald Horn. Modelling the energy balance of an anaerobic digester fed with cattle manure and renewable energy crops. *Water Research*, 41(18):4085–4096, 2007.

[48] Eric Mauky, Sören Weinrich, Hans-Joachim Nägele, H Fabian Jacobi, Jan Liebetrau, and Michael Nelles. Model predictive control for demand-driven biogas production in full scale. *Chemical Engineering & Technology*, 39(4):652–664, 2016.

[49] D. Q. Mayne, E. C. Kerrigan, E. J. van Wyk, and P. Falugi. Tube-based robust nonlinear model predictive control. *International Journal of Robust and Nonlinear Control*, 21(11):1341–1353, 2011.

[50] Rongrong Mo, Wenjie Guo, Damien Batstone, Jacek Makinia, and Yongmei Li. Modifications to the anaerobic digestion model no. 1 (adm1) for enhanced understanding and application of the anaerobic treatment processes – a comprehensive review. *Water Research*, 244:120504, 2023.

[51] Modelica Association. *Modelica—A Unified Object-Oriented Language for Systems Modelling, Language Specification, Version 3.3*. Modelica Association, 2012.

[52] E. Morel, B. Tartakovsky, S.R. Guiot, and M. Perrier. Design of a multi-model observer-based estimator for anaerobic reactor monitoring. *Computers & Chemical Engineering*, 31(2):78–85, 2006.

[53] H.O. Méndez-Acosta, B. Palacios-Ruiz, V. Alcaraz-González, V. González-Álvarez, and J.P. García-Sandoval. A robust control scheme to improve the stability of anaerobic digestion processes. *Journal of Process Control*, 20(4):375–383, 2010.

[54] Emil Petre, Dan Selişteanu, and Dorin Şendrescu. Adaptive and robust-adaptive control strategies for anaerobic wastewater treatment bioprocesses. *Chemical Engineering Journal*, 217:363–378, 2013.

[55] Ennio R. Piceno-Díaz, Luis A. Ricardez-Sandoval, Miguel A. Gutierrez-Limon, Hugo O. Méndez-Acosta, and Héctor Puebla. Robust nonlinear model predictive control for two-stage anaerobic digesters. *Industrial & Engineering Chemistry Research*, 59(52):22559–22572, 2020.

[56] Andrés Pino Santana, Santiago Garcia-Gen, Laurent Dewasme, and Alain Vande Wouwer. Model predictive control of anaerobic digestion processes using a long short-term memory network predictor. *Water Science and Technology*, 92(7):1063–1076, 09 2025.

[57] Lingga Aksara Putra, Bernhard Huber, and Matthias Gaderer. Real-world application of a discrete feedback control system for flexible biogas production. *Advanced Modeling and Simulation in Engineering Sciences*, 10(1):16, 2023.

[58] Niloofar Raeyatdoost, Michael Bongards, Thomas Bäck, and Christian Wolf. Robust state estimation of the anaerobic digestion process for municipal organic waste using an unscented kalman filter. *Journal of Process Control*, 121:50–59, 2023.

[59] L E Ripley, W C Boyle, and J C Converse. Improved alkalimetric monitoring for anaerobic digestion of high-strength waste. *J. - Water Pollut. Control Fed.; (United States)*, 58:5, 05 1986.

[60] A. Rodríguez, G. Quiroz, R. Femat, H.O. Méndez-Acosta, and J. de León. An adaptive observer for operation monitoring of anaerobic digestion wastewater treatment. *Chemical Engineering Journal*, 269:186–193, 2015.

[61] Christian Rosén and Ulf Jeppsson. *Aspects on ADM1 Implementation within the BSM2 Framework*, volume 7224 of *TEIE*. Department of Industrial Electrical Engineering and Automation, Lund Institute of Technology, 2005.

[62] Juan G. Rueda-Escobedo, Mihaela Sbarciog, Jaime A. Moreno, Jan Van Impe, and Alain Vande Wouwer. Robust state and input estimation with enhanced convergence rate for monitoring anaerobic digestion. *Journal of Process Control*, 117:169–180, 2022.

[63] Guglielmo Santi, Simona Proietti, Stefano Moscatello, Walter Stefanoni, and Alberto Battistelli. Anaerobic digestion of corn silage on a commercial scale: Differential utilization of its chemical constituents and characterization of the solid digestate. *Biomass and Bioenergy*, 83:17–22, 2015.

[64] M. Sbarciog, J. A. Moreno, and A. Vande Wouwer. Application of super-twisting observers to the estimation of state and unknown inputs in an anaerobic digestion system. *Water Science and Technology*, 69(2):414–421, 11 2013.

[65] Hansruedi Siegrist, Dea Vogt, Jaime L. Garcia-Heras, and Willi Gujer. Mathematical model for meso- and thermophilic anaerobic sewage sludge digestion. *Environmental Science & Technology*, 36(5):1113–1123, 2002. PMID: 11917999.

[66] Atthasit Tawai and Malinee Sriariyanun. Nonlinear optimization-based robust control approach for a two-stage anaerobic digestion process. *Journal of Chemistry*, 2022(1):8966350, 2022.

[67] Jin M. Triolo, Sven G. Sommer, Henrik B. Møller, Martin R. Weisbjerg, and Xin Y. Jiang. A new algorithm to characterize biodegradability of biomass during anaerobic digestion: Influence of lignin concentration on methane production potential. *Bioresource Technology*, 102(20):9395–9402, 2011.

[68] Katarzyna Waszkielis, Ireneusz Białobrzewski, and Katarzyna Bułkowska. Application of anaerobic digestion model no. 1 for simulating fermentation of maize silage, pig manure, cattle manure and digestate in the full-scale biogas plant. *Fuel*, 317:123491, 2022.

[69] Sören Weinrich and Michael Nelles. *Basics of Anaerobic Digestion - Biochemical Conversion and Process Modelling*. DBFZ Deutsches Biomasse Forschungs Zentrumgemeinnützige GmbH, Leipzig, Germany, 05 2021.

[70] Sören Weinrich and Michael Nelles. Systematic simplification of the anaerobic digestion model no. 1 (adm1) – model development and stoichiometric analysis. *Bioresource Technology*, 333:125124, 2021.

[71] F. Weißbach and C. Strubelt. Correcting the dry matter content of maize silages as a substrate for biogas production. *Landtechnik*, 63(2):82–83, 2008.

[72] Bernhard Wett, A Eladawy, and Michael Ogurek. Description of nitrogen incorporation and release in adm1. *Water science and technology : a journal of the International Association on Water Pollution Research*, 54:67–76, 02 2006.

[73] Sihuang Xie, Faisal I. Hai, Xinmin Zhan, Wenshan Guo, Hao H. Ngo, William E. Price, and Long D. Nghiem. Anaerobic co-digestion: A critical review of mathematical modelling for performance optimization. *Bioresource Technology*, 222:498–512, 2016.

[74] Lei Xue, Dewei Li, and Yugeng Xi. Nonlinear model predictive control of anaerobic digestion process based on reduced adm1. In *2015 10th Asian Control Conference (ASCC)*, pages 1–6, 2015.

[75] Kazuto Yoshida and Naoto Shimizu. Biogas production management systems with model predictive control of anaerobic digestion processes. *Bioprocess and Biosystems Engineering*, 43(12):2189 – 2200, 2020.

[76] Haidong Zhou, Zhenxi Ying, Zhengcao Cao, Zhiyong Liu, Zhe Zhang, and Weidong Liu. Feeding control of anaerobic co-digestion of waste activated sludge and corn silage performed by rule-based pid control with ADM1. *Waste Management*, 103:22–31, 2020.